

Hunting for Substructure in the Milky Way

Melissa Harris

Lund Observatory
Lund University



2015-EXA98

Degree project of 15 higher education credits
May 2015

Supervisor: Gregory Ruchti

Lund Observatory
Box 43
SE-221 00 Lund
Sweden

Abstract

Studies of the Milky Way including how it formed and evolved through time are the key to understanding how other galaxies behave. The Milky Way is the most convenient galaxy to study, because the close proximity of stars means astronomers can collect precise spectral and dynamical data from individual stars. By combining the chemical and dynamical aspects, it is possible to pinpoint stars which have been accreted from satellite galaxies, in comparison to stars which formed in situ. This constrains the merger history of the Milky Way, which is an important factor in understanding how it has evolved since its formation.

In this thesis I have performed a chemodynamical analysis of two sets of data; Fulbright and Nissen & Schuster. I analysed abundance ratios of $[\text{Mg}/\text{Fe}]$ and $[\text{Ni}/\text{Fe}]$ relative to $[\text{Fe}/\text{H}]$ to indicate which stars could be accreted. I then calculated the specific angular momentum, which is the z-component of angular momentum, normalised to a circular orbit: J_z/J_c . I also calculated the specific energy, which is the z-component of the energy, also normalised to a circular orbit: E_z/E_c . From these calculations I analysed the orbits of the stars to predict which stars could be accreted. Subsequently, I combined the two methods into the chemodynamical analysis to identify with confidence how many stars from each sample are accreted. From the Fulbright sample, I successfully identified 18 out of 167 stars which were accreted. From the Nissen & Schuster sample, I successfully identified 29 out of 100 stars which were accreted. These accreted stars are from mergers of low mass dwarf galaxies with the Milky Way, and provide evidence of substructure in the Milky Way.

Jakten på substrukturer i Vintergatan

–ett försök att förstå galaxens historia genom tolkning av ovanliga strömmar av stjärnor

För oss människor här på jorden har det alltid varit svårt att föreställa sig vår vidsträckta galax, Vintergatan, som får vår planet att framstå som så liten. Med blicken upp mot Vintergatan kan många frågor väckas; hur formades galaxen? Hur har den förändrats med tiden? Vad är det som bestämmer hur den beter sig? Dessa och många andra frågor försöker 2000-talets astronomer finna svar på. Men kommer vi någonsin att kunna lösa mysteriet bakom en galax vars historia sträcker sig flera miljarder år tillbaka i tiden?

Lyckligt nog finns det ledtrådar gömda bland stjärnorna runt omkring oss. När en stjärna föds minns den vilka ämnen den formades från och längs vilken bana den rörde sig. Än idag kan kartläggningen av en stjärna ge tillgång till den här informationen och ge oss ett kikhål till det förflutna. Genom att skicka ut nutidens moderna teleskop i rymden och låta dem granska stjärnorna kan vi på så sätt närma oss svaren på våra frågor. Astronomerna samlar sedan ihop all information för att till slut kunna beskriva hur vår galax har expanderat och utvecklats genom tiden och antagit den skepnad vi ser idag.

Den här metoden tycktes ha löst mysteriet, ända tills teleskopen och astronomerna stötte på en stjärna som såg lite annorlunda ut. Den verkade inte riktigt passa in. Den kanske bestod av andra ämnen än stjärnorna runt omkring? Eller rörde den sig i ett kretslopp vi inte hade förväntat oss? Faktum är att dessa typer av stjärnor har påträffats över hela galaxen. Orsaken till att de skiljer sig från Vintergatans flesta stjärnor är förvånansvärt uppenbar: de kommer ursprungligen inte från Vintergatan. De har kommit från andra håll. Andra galaxer kan nämligen ströva för nära eller till och med krocka med Vintergatan så att stjärnor slits bort från dem och dras in i vår galax där de blandar sig med stjärnor som funnits här sedan länge.

På så sätt lockar Vintergatan oss med strömmar och strömmar av stjärnor som viskar om spår av helt andra galaxer. Dolt bland de ursprungliga strukturerna ligger en fascinerande substruktur som berättar om de gånga händelser där vår galax har förvärvat främmande stjärnor. Just den här aspekten är den centrala idén till min uppsats, där jag ska leta efter de främmande stjärnorna och på egen hand jaga efter substrukturer i Vintergatan.

Contents

1	Introduction	2
1.1	Chemical analysis of stars	4
1.1.1	Absorption Spectra	4
1.1.2	Metallicity	4
1.1.3	Abundance Plots	5
1.1.4	Supernovae classification	5
1.1.5	Interpreting abundance plots	6
1.2	Dynamical Analysis	9
1.2.1	Structure of the Milky Way	9
1.2.2	Coordinates and Velocities of Stars	9
1.2.3	Galactic Potential	9
1.2.4	Orbits of stars	10
1.3	Chemodynamical Analysis	12
1.3.1	Mergers	12
1.3.2	Radial Migration	13
1.3.3	Evidence of accretion	13
1.4	Method	14
1.4.1	Data Sets	14
2	Results	18
2.1	Abundance Plots	19
2.1.1	Fulbright Data Set	19
2.1.2	Nissen and Schuster Data Set	21
2.2	Orbits Plots	23
2.2.1	Fulbright Data Set	23
2.2.2	Nissen and Schuster Data Set	24
2.3	Chemodynamical Analysis	25
2.3.1	Fulbright Data Set	26
2.3.2	Nissen and Schuster Data Set	31
3	Conclusion	37
A	Matrix Calculations for velocities	42

Chapter 1

Introduction

Astronomers want to understand how galaxies form and how they evolve over time. The best way to do this is to study our own Galaxy, the Milky Way. Assuming that the Milky Way is a typical galaxy, the concepts can then be applied to other galaxies. The main advantage to this method is that the stars in our Galaxy are the closest to Earth, which means that data from individual stars can be collected and analysed. The Milky Way is the only galaxy where it is possible to study the kinematics and chemistry of all types of stars, probing all stellar components in the Galaxy. It is not possible to do this for any other galaxy because they are too far away. Previous surveys of chemical and dynamical data include the Radial Velocity Experiment (Steinmetz et al. 2006), *Hipparcos* (Eyer et al. 2012) and the *Gaia-ESO* survey (Gilmore et al. 2012).

There are two main methods to study stars; spectral analysis and dynamical analysis. Spectral analysis means studying the elements present in the atmospheres of stars, and calculating relative abundances of certain elements. Dynamical analysis means looking at the orbits on which the stars move. Combining information from both methods is called chemodynamical analysis and gives the best picture of the star's history, and subsequently the history of the Milky Way.

Studies are based on the principle that old, low mass stars retain information from the past, including when and where they formed. A star forms in the interstellar medium of the Galaxy which is rich in certain elements. The types and amounts of elements are dependent on supernova explosions. There are two main types of supernovae which enrich the interstellar medium with different amounts of high mass elements. When a new low mass star forms, its atmosphere contains these elements and retains them for many years. Spectra from stars give information about the elements in the stars' atmospheres. Therefore, from the spectra of stars we can obtain knowledge about the Galaxy many years ago when the star formed.

Furthermore, when a star forms in the Galactic disc, it moves in an approximately circular orbit due to the axisymmetric potential from the massive centre of the Galaxy and

the surrounding stars. This means that the angular momentum is predominantly in the direction of the North Galactic Pole. In order to conserve angular momentum, over time this orbit remains approximately circular. Astronomers measure the velocity and distances of stars to analyse the angular momentum, and from this they can determine how circular the orbit of each star is.

In previous years, astronomers had a simple outlook on the structure of our Galaxy, which has evolved over time with ongoing research in the area. At its most basic level, the Milky Way is a barred disk galaxy with spiral arms. Its main components are the central bulge, the disk and the surrounding halo. When analysed in further detail, the disk can be divided into two components; a thin disc and a thick disk. There is no definitive distinction between these two structures; when dynamical and chemical properties of stars in both are analysed there is much overlap. Therefore, some astronomers believe that no such distinction between the thick disk and the thin disk can be made. See Bovy et al. (2012) and Reddy et al. (2006) for two opposing views. Assuming that we can divide the disk in this way, our Sun is located in the thin disk of the Milky Way.

The different components of the Milky Way contain stars with properties typical to it; i.e stars in the thin disk show a certain trend, which in general differs from stars in the thick disk. The halo and bulge also contain stars with characteristic properties. Therefore, when stars which formed in the thin disk are analysed, they are likely to show spectral and dynamical properties typical of the thin disk. For some stars this is not the case. Therefore, it is possible that the star migrated from a different part of the Galaxy, or alternatively formed in a different galaxy entirely which later merged with the Milky Way. These accreted stars from merger events form substructure within the Milky Way, which is hidden amongst the stars which formed 'in situ'.

In this study, I have extracted previously taken spectral and dynamical data for stars in the Solar neighbourhood. The positions of the stars were originally recorded by the *Hipparcos* satellite. Initially, I studied the spectral properties and dynamical properties separately. Finally, I combined the two methods into a chemodynamical study in an attempt to find evidence of accreted stars in my two samples. Evidence of accreted stars is therefore proof that there is substructure in the Milky Way.

1.1 Chemical analysis of stars

Astronomers want to study the history of the Milky Way and how it has evolved over time, otherwise termed 'Galactic Archaeology' (e.g. Freeman & Bland-Hawthorn 2002). This is achieved by chemical analysis of stellar populations, (e.g. Snaith et al. 2014; Bensby et al. 2014). Signatures of the Galaxy's past are retained in the atmospheres of stellar populations. Absorption spectra from stars give us the relative abundances of certain elements. Studying these abundances indicates the age of a star and whether the star has properties typical of the Milky Way. From this, one can make predictions about whether the star originally formed in the Milky Way. If this is not the case, then it is possible that the star has come from a satellite galaxy outside the Milky Way. These accreted stars form substructure inside the Galaxy. This section includes an overview of the theory necessary to perform a chemical analysis of a stellar population.

1.1.1 Absorption Spectra

The interstellar medium of a galaxy becomes enriched in various elements over time. When a new star forms, the amount of these elements remains fairly constant in the atmosphere of the star. Astronomers can gain information about a star from its absorption spectrum. Light from the star passes through the star's atmosphere and absorption lines in the spectrum indicate which elements are present in the atmosphere. These are therefore the elements which were present in the galaxy when the star originally formed. Catalogues such as the Radial Velocity Experiment contain data about the relative abundances of elements, particularly metals.

1.1.2 Metallicity

One useful method of analysing a star is by calculating its metallicity. In particular the metal content can serve as a first guess for the age of a star. In stellar spectroscopy, a metal is any element X with a higher atomic number than helium. The metallicity is defined as the ratio of metals compared to hydrogen, given relative to the sun.

$$[X/H] \equiv \log \left(\frac{n(X)}{n(H)} \right)_* - \log \left(\frac{n(X)}{n(H)} \right)_\odot \quad (1.1)$$

In equation 1.1, $n(X)$ is the number density of element X. In this study, the term metallicity relates specifically to the abundance of iron relative to hydrogen, i.e. $[\text{Fe}/\text{H}]$.

Alternatively, the ratio of a different metal, X, is often calculated relative to iron rather than hydrogen. This $[X/\text{Fe}]$ is referred to as the abundance of the metal X, not to be confused with metallicity. These metal abundances will be explained further in later sections.

1.1.3 Abundance Plots

Knowledge of a star's history can be gained by analysing the relative abundances of various elements in its atmosphere. Equation 1.1 is used to calculate $[\text{Fe}/\text{H}]$ for a star, which is plotted on the x-axis. The abundance of a particular metal such as an α element (see 1.1.4) relative to iron is denoted $[\alpha/\text{Fe}]$ and is plotted on the y-axis.

Abundance plots therefore show how the relative amount of a particular metal changes with respect to the amount of iron in the atmosphere of a star. The graphs show particular trends which will be analysed later, which relate to the ages of stars and the star formation history of a stellar sample. As the metallicity equation gives values relative to solar values, the point (0,0) on an abundance plot represents the Sun.

The abundances of both alpha elements and iron can be explained by supernovae explosions, which is explained in the following section.

1.1.4 Supernovae classification

Supernovae are luminous stellar explosions which can be categorised into different types based on how they occur. There are several different types, however here it is important to name two categories; core collapse and type Ia. The theory behind both types was taken from Schneider (2015).

Type Ia Supernovae

Type Ia supernovae are exploding white dwarf stars. A star exhibits a balance between the gravitational force causing it to collapse, and the pressure due to fusion and electron degeneracy, opposing the collapse. There is a critical mass above which the pressure can no longer significantly oppose the gravitational force. This so called Chandrasekhar mass is $\approx 1.44M_{\odot}$. White dwarf stars which are more massive than this become unstable and explode.

There are two ways in which a white dwarf can lead to a supernova explosion. In one case, a white dwarf that is part of a binary system can slowly accrete material from its partner until it reaches the critical mass. After this, the more massive white dwarf explodes and the iron which was produced inside it via nuclear fusion is deposited in the interstellar medium. In the alternative case, two white dwarfs merge together, producing a combination with sufficient mass for an explosion, depositing iron from both stars into the galaxy.

As a general rule, type Ia supernovae begin to explode approximately 1 Gyr after the stellar population formed, although this is a rough guide and can vary. More importantly, type Ia supernovae take longer to occur than core collapse supernovae, which are explained

in the next section.

Core Collapse Supernovae

Core collapse is a general category to describe type II, type Ib and Ic supernovae. They occur when massive stars (above approximately $8 M_{\odot}$) can no longer oppose the gravitational force caused by their mass, and become unstable and collapse.

As part of the life cycle of a star, nuclear fusion produces increasingly heavy elements. Iron has the highest binding energy per nucleon, meaning once it is being produced, no more energy can be produced from fusion. At this stage, the star collapses to a dense core, heating the infalling material, so that it bounces off the core and into the interstellar medium. The remaining dense core can become a neutron star or a black hole.

The metals which are ejected from exploding supernovae into the interstellar medium can then become part of newly forming stars. Stellar fusion produces an abundance of metals with even numbers of protons and neutrons, called the α elements: C, O, Ne, Mg, Si, Ca; as well as the so-called iron peak elements with $21 \leq Z \leq 28$, (Suda et al. 2011) such as Ti, Fe and Ni. Core collapse supernovae typically begin to explode $\sim 10^7$ years after a galaxy forms.

1.1.5 Interpreting abundance plots

Star Formation Efficiency

The metallicity and metal abundances of stars can be linked to their star formation history. Before a galaxy forms, the area is assumed to have low metallicity and low metal abundances. Later, supernova explosions enrich the interstellar medium with elements which subsequently are present in newly forming stars. Core-collapse supernovae explode first, around 10^7 years after a galaxy has formed. This enriches the interstellar medium with alpha elements and iron. Therefore, when new stars form from the debris, the the ratio of the alpha elements to iron abundance remains fairly constant in their atmospheres, while the iron abundance steadily increases.

After some time, the white dwarf stars begin to explode as type Ia supernovae, enriching the interstellar medium with iron, but little to no alpha elements. Therefore, the ratio of alpha elements to iron will decrease in newly formed stars' atmospheres.

For some time after formation, a galaxy remains active and continues to form new stars, a number of which result in core collapse supernovae. Therefore, there is a balance between the alpha abundance $[\alpha/\text{Fe}]$ and the metallicity $[\text{Fe}/\text{H}]$ of stars. At this stage, the galaxy is referred to as having a strong star formation efficiency, see Tolstoy et al. (2009). In an abundance plot of $[\alpha/\text{Fe}]$ against $[\text{Fe}/\text{H}]$, there is a plateau indicating this. For example of

this plateau, see Figure 1.1, Milky Way stars $\sim -2 < [\text{Fe}/\text{H}] < -0.8$.

Eventually, the iron from type Ia supernovae begins to dominate the elemental abundance in new stars. At this point, there is a so called 'knee' in the abundance plot, where the alpha abundance drops fairly abruptly. The higher the star formation efficiency of a galaxy, the higher metallicity the galaxy reaches before the $[\alpha/\text{Fe}]$ ratio decreases and this knee occurs. For an example of the 'knee', see Figure 1,1, Milky Way stars at $[\text{Fe}/\text{H}] \sim -0.8$.

Determining the origin of a star from abundance plots

With an understanding of how the star formation efficiency of a stellar population affects its abundance plot, it becomes possible to determine the origin of a star. To demonstrate this, an abundance plot taken from previous research in alpha abundances in a study by Ruchti et al. (2014) is given below. Figure 1.1 demonstrates the typical $[\text{Mg}/\text{Fe}]$ abundance

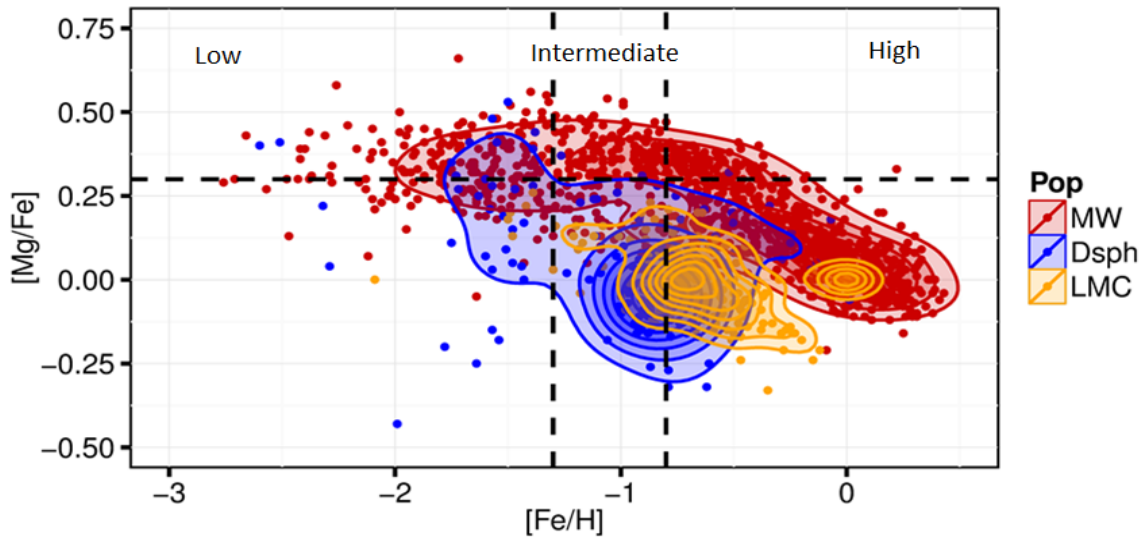


Figure 1.1: $[\text{Mg}/\text{Fe}]$ against $[\text{Fe}/\text{H}]$ abundance plot taken from Ruchti et al. (2014), for each stellar population: Milky Way, a typical dwarf spheroidal galaxy and the LMC. There are cuts in the metallicity at $[\text{Fe}/\text{H}] = -0.8$ and -1.3 . There is an additional cut in the $[\text{Mg}/\text{Fe}]$ abundance at $[\text{Mg}/\text{Fe}] = 0.3$.

plot trend for several stellar populations, each with a different star formation history. In the study by Ruchti et al. (2014), a model was used to simulate the evolution of the Milky Way, a small dwarf spheroidal galaxy (Dsph) and the LMC. The resulting $[\text{Mg}/\text{Fe}]$ against $[\text{Fe}/\text{H}]$ relation demonstrates the use of a chemical analysis. Whilst the study used simulations for the dynamics of the stars, the abundances plotted in Figure 1.1 are observed elemental abundance ratios measured in the Milky Way and other satellite galaxies.

For the analysis of accreted stars in this thesis, it is helpful to refer to the Milky Way stars and the Dsph stars. As the Milky Way is much more massive and rich in elements, it consequently exhibits a strong star formation efficiency. Therefore, the stars reach a higher metallicity before the knee occurs. It is clear from Figure 1.1 that stars from a smaller dwarf galaxy typically lie at lower metallicity values. This is a consequence of the lower star formation efficiency.

The graph is separated into three bins of metallicity. The high metallicity bin defines the stars with $[\text{Fe}/\text{H}] > -0.8$. The intermediate metallicity bin defines stars with $-1.3 < [\text{Fe}/\text{H}] < -0.8$. Finally, the low metallicity bin defines stars with $[\text{Fe}/\text{H}] < -1.3$. In each bin, the $[\text{Mg}/\text{Fe}]$ values of the Milky Way can be compared to those of a Dsph.

In the high metallicity bin, there are fewer stars from the dwarf galaxy, and it is clear that the dwarf galaxy doesn't reach as high a metallicity as the Milky Way. In this region, the Milky Way stars are typical of thin disc stars (Schneider 2015).

Furthermore, in the intermediate metallicity bin, the dwarf galaxy stars typically have lower $[\text{Mg}/\text{Fe}]$ abundances than those of the Milky Way. This is due to the difference in star formation efficiency.

In the lowest metallicity bin, the dwarf galaxy stars exhibit similar $[\text{Mg}/\text{Fe}]$ abundances to the Milky Way stars, making it more difficult to distinguish between them. For the Milky Way, this region of the abundance plot indicates that the stars are typical of the thick disc or the halo (Schneider 2015).

Figure 1.1 demonstrates how useful an abundance plot can be in determining the origin of a star. In particular for this study, it is possible to search for accreted stars from dwarf galaxies, by looking for low $[\text{Mg}/\text{Fe}]$ abundances at intermediate metallicity values.

Limitations of a purely chemical analysis

This section has indicated how a chemical analysis can be used to identify accreted stars which are currently present in the Milky Way but originated in a dwarf galaxy. However, the analysis is not without limitations. From the chemistry alone, one can't know whether a star has in fact been accreted from a dwarf galaxy, or if it has formed in the Milky Way and later migrated to a different part of the Milky Way. Typically, the halo and thick disc consist of stars with higher $[\text{Mg}/\text{Fe}]$ abundances than the thin disc, although there is definite overlap. Therefore, to distinguish between true accreted stars and in situ stars, a dynamical analysis is also required. This will be explored in the following section.

1.2 Dynamical Analysis

1.2.1 Structure of the Milky Way

At a basic level, the Milky Way consists of the central bulge, the disk and the stellar halo. The disc is a band of stars containing spiral arms, and is often split into two components; the thick disk and the thin disk. The halo is an approximately spherical distribution of stars and globular clusters which surrounds the disk. The Sun is situated roughly 8 kpc from the Galactic Centre and is a part of the thin disk (Schneider 2015).

1.2.2 Coordinates and Velocities of Stars

Stars in the Milky Way are defined by their positions and velocities. It is useful to know how stars move relative to the Galactic Centre and the North Galactic Pole. Satellites such as *Hipparcos* provide the coordinates of the stars. They provide the parallaxes which are required to calculate the distance to the stars. This is needed to derive the proper motions and radial velocities of the stars. The radial velocities are measured from the Doppler shifts of spectral lines, where a positive velocity defines a star which is moving away from Earth. The proper motions are the angular velocities in the directions of right ascension and declination. These are measured in arcseconds per year.

It is more convenient to convert from the radial velocities and proper motions which we measure directly into velocities in a cylindrical coordinate system with the Sun at the origin. These are denoted U , V and W . The velocity towards the Galactic centre is U , the tangential velocity is V and the velocity towards the North Galactic Pole is W . All are measured in km/s. The transformation into these U , V and W values is done using matrix calculations, which are included in Appendix A.

As the U , V and W velocities have the Sun as the origin, there needs to be a correction to take into account the fact that stars in a sample are often a short distance away from the Sun. This is a simple addition of values to each of U , V and W . These values are the solar motion relative to the local standard of rest (LSR), and are: (14.0, 12.24, 7.25) taken from (U : Schönrich (2012), V and W : Schönrich et al. (2010)). In addition to this, the tangential velocity at the radius of the Sun needs to be added to the V component to take into account the rotation about the galaxy. This value is widely accepted to be 220 km/s.

1.2.3 Galactic Potential

The orbit that a star moves on is determined by the Galactic potential. The potential is calculated by fitting models of stellar and dark matter distributions to observations. There is an equation for each of: bulge, disk and halo. These three potentials were taken from Gómez et al. (2010).

The bulge potential is given by:

$$\Phi_{bulge}(R, z) = \frac{-GM_b}{\sqrt{R^2 + z^2 + r_c}}. \quad (1.2)$$

The disc potential is given by:

$$\Phi_{disc}(R, z) = \frac{-GM_d}{\sqrt{R^2 + (r_a + \sqrt{z^2 + r_b^2})^2}}. \quad (1.3)$$

The dark matter halo is given by:

$$\Phi_{halo}(R, z) = \frac{-GM_{vir}}{\sqrt{R^2 + z^2}[\log(1+c) - c/(1+c)]} \log\left(1 + \frac{\sqrt{R^2 + z^2}}{r_s}\right) \quad (1.4)$$

The addition of equations 1.2, 1.3 and 1.4 provides the total potential at any point in the Galaxy. The potential influences the orbit of each star, in addition to the energy of the star. These aspects will be explored further in section 1.2.4.

1.2.4 Orbits of stars

Angular Momentum and Energy

Stars move on their orbits in the Milky Way with an angular momentum vector, which is the cross product between the radius R from the Galactic centre and the tangential velocity, V . For a circular orbit, this momentum points in the direction of the North Galactic Pole. Therefore, to assess the orbits of stars it is helpful to consider the z -component of angular momentum, J_z , which is the component pointing towards the North Galactic Pole.

$$J_z = RV \quad (1.5)$$

The total energy of a star is calculated from the kinetic energy and the Galactic potential at its R, z position. This is given by equation 1.6.

$$E_{tot} = \frac{U^2 + V^2 + W^2}{2} + \Phi(R, z) \quad (1.6)$$

In order to indicate how circular the orbit of a star is, it is useful to normalise the angular momentum relative to a star on a purely circular orbit. This method was inspired by the paper Ruchti et al. (2014). For each star, we take a hypothetical star with the same E_{tot} , but moving on a circular orbit, and calculate the radius R_c of this orbit. This requires a minimisation of equation 1.7, which can be done using a program such as R which has a minimisation function.

$$\left| \frac{V_c^2}{2} + \Phi(R_c, 0) - E_{tot} \right| \quad (1.7)$$

where the circular velocity V_c is given by

$$V_c = \sqrt{R_c \frac{\partial \Phi}{\partial R} \Big|_{R=R_c}} \quad (1.8)$$

The angular momentum corresponding to this hypothetical circular orbit is denoted J_c , and is calculated from equation 1.9.

$$J_c = R_c V_c. \quad (1.9)$$

The normalised angular momentum, referred to as the specific angular momentum, is then the ratio of J_z to J_c . The specific angular momentum therefore lies between -1 and 1 and indicates how circular the orbit of the star in question is. A value of 1 indicates a circular orbit, whilst a negative value indicates a retrograde orbit.

In addition, a specific energy can be calculated for each star. Again, the z-component is calculated, which is given in equation 1.10.

$$E_z = \frac{W^2}{2} + \Phi(R, z). \quad (1.10)$$

The specific energy is the ratio of E_z to E_c , where circular energy is the energy of the star on a circular orbit, given by

$$E_c = \Phi(R, 0). \quad (1.11)$$

The specific energy of the star indicates how far out of the plane a star is moving.

Predicting the origin of a star from angular momentum and energy

Once the specific angular momentum and energy of a star are known, it becomes possible to predict the origin of the star. The principle behind this is that a new star forms in the disc on a circular orbit due to the symmetry of the Galactic potential. The star then remains on this circular orbit in the Milky Way throughout its lifetime. However, a star that has been accreted from a dwarf galaxy into the Milky Way will not be on a circular orbit. This distinction makes it possible to identify accreted stars. The theory behind merger events will be discussed further in the chemodynamical analysis in section 1.3.

Limitations of a purely dynamical analysis

Although a dynamical analysis gives an insight into finding accreted stars, it doesn't give the entire picture. In the same way as a chemical analysis, by looking purely at the orbits of stars, the outcome can be misleading. For example, stars in the Milky Way halo do not move on particularly circular orbits, so they could be mistaken for accreted stars. Furthermore, stars from a massive merger have a higher J_z/J_c value than stars from a small merger with a dwarf galaxy. Therefore, it is necessary to take both the dynamics and the chemistry into account to gain a full understanding of accreted stars. This will be explained in detail in section 1.3.

1.3 Chemodynamical Analysis

To confidently identify substructure in the Milky Way it is not sufficient to analyse purely chemical data or purely dynamical data. However, by combining both methods one can gain the best insight to the history of a stellar population. This is called chemodynamical analysis. By studying both the spectra of a population and the orbits that the stars move on, it becomes possible to identify which have been accreted. It is these accreted stars which form the substructure. In this section, the merger events which lead to accreted stars will be explained. Furthermore, the method behind finding accreted stars will be outlined. This chemodynamical analysis is the method used to find accreted stars in my data sets.

1.3.1 Mergers

It is believed that Λ cold dark matter galaxies such as the Milky Way experience many mergers with other stellar populations over their lifetimes. The Milky Way halo is sensitive to accretion of low mass satellites, in contrast to the Milky Way disc which is most sensitive to accretion of massive satellites (e.g. Ruchti et al. 2014).

Mergers with small dwarf galaxies

When smaller satellite galaxies merge with the Milky Way, their debris is deposited across the Milky Way halo. These streams of stars from external galaxies give the substructure which astronomers are searching for. These accreted stars have characteristically low J_z/J_c and E_z/E_c values, meaning they move on non-circular orbits, far out of the plane. Often the specific angular momentum lies near to zero or at negative values, indicating that the orbits are retrograde.

Mergers with massive galaxies

When massive satellite galaxies merge with the Milky Way, there are two signature effects. The first is that the Milky Way disc becomes hot, leading to an increase in height of the disc as its shape warps due to the heat and stars migrate radially outwards. See Kazantzidis et al. (2008) for a numerical simulation proving this. The second signature is that a frictional force drags the satellite into the plane of the Milky Way (Read et al. 2008) where the galaxy is stripped tidally and deposits its stars in an accreted disc (not to be confused with the Milky Way's own thin or thick disc). These accreted stars from massive galaxies also have J_z/J_c and E_z/E_c values below 1, however, they are not as low as those for a small merger. This is due to the frictional force dragging the massive merger stars onto more circular orbits than those from a small merger. As a consequence, it is more difficult to identify stars from a massive merger, because their orbits are less radical. Furthermore, their abundances are closer to those of in situ Milky Way stars. Therefore, previous research to identify stars from a massive merger have not succeeded, suggesting

the Milky Way has experienced no large mergers since the disc formed, see Ruchti et al. (2015).

1.3.2 Radial Migration

In some cases, stars might be mistaken for accreted stars when they in fact formed in a different part of the Milky Way. Stars can receive a 'kick' from the spiral arms of the Milky Way, causing them to move to a smaller radius. If the star originally formed in the Milky Way then it will originally move on a spherical orbit. After the kick, the circularity of the orbit will not change significantly, to conserve angular momentum. Therefore one can distinguish between accreted stars from a small dwarf galaxy and stars which radially migrated from a different part of the Milky Way; the former move on significantly non-spherical orbits and the latter move on spherical orbits.

1.3.3 Evidence of accretion

Previous experimental and Computational evidence

After accepting that the Milky Way contains accreted stars from dwarf galaxies, the subsequent step is to explore the consequences of the mergers and find evidence. Research in the area of mergers and accretion involves both simulations of hypothetical mergers and experimental observations of stars in the Milky Way. One example of experimental evidence is the tidal stream from the Sagittarius dwarf galaxy, a spheroidal dwarf galaxy being tidally shredded and absorbed into the Milky Way (e.g. Ibata et al. 1994; Newberg et al. 2002). In simulations, models used to describe mergers are based on a Λ cold dark matter model of the universe, which is based on the thermal velocity of matter in the universe, and affects how the universe evolves in time. An example of a simulation of an accretion event is Lokas et al. (2011).

Using chemodynamics to find accreted stars

During a merger, stars, gas and dark matter are stripped from the satellite and deposited in the Milky Way amongst those which formed in situ and were already present. It is therefore possible to look for evidence of accretion by finding stars in the Milky Way which likely originated in another galaxy. Therefore, the resulting substructure can teach astronomers about the merger history of the Milky Way.

The abundance plots described in 1.1.3 give the first clue to finding accreted stars. For a stellar sample, an $[\alpha/\text{Fe}]$ against $[\text{Fe}/\text{H}]$ relation can be plotted. Any stars in the sample with uncharacteristically low abundances are then possible accreted stars. When the orbits of these stars are also analysed, the stars which are definitely accreted can be identified. Studies such as Tolstoy et al. (2009) have shown that dwarf galaxies neighbouring the Milky Way at metallicities greater than -1.5 generally have low $[\alpha/\text{Fe}]$ values compared to the Milky Way. This can be understood by resorting back to the theory in 1.1.5. As the

Milky Way stars have higher $[\alpha/\text{Fe}]$ values, this indicates the star formation efficiency is higher, as expected for a large, active galaxy. In contrast, a small dwarf spheroidal galaxy's star formation efficiency dwindles on a shorter time scale, explaining the lower ratio of α elements to iron. Resort back to Figure 1.1 for a visualisation of this.

However, as outlined in 1.1.5 and 1.3.2, stars with abnormal abundances could have migrated from a different part of the Milky Way. In this case, the orbit of the star will be circular, which rules out the possibility of the star being accreted.

In conclusion, the overall principle of a chemodynamical analysis is as follows. Stars in the Milky Way with abundances typical of small dwarf galaxies are identified. The orbits of these stars are then analysed to extract the stars moving on non-circular orbits. The remaining stars are therefore proven to be accreted. This is the method used for the data sets in this thesis, which will be explained in section 1.4.

1.4 Method

For my investigation into finding the substructure of accreted stars, I analysed data taken from two sources; Nissen & Schuster (Nissen & Schuster 2010) and Fulbright (Fulbright 2000, 2002). In addition to this, I extracted data from the Simbad online catalogue. The stars in these two samples were selected from the *Hipparcos* catalogue, which provides parallax measurements, which can be used to derive the distance to the stars. High-resolution spectra were obtained in each work in order to measure the elemental abundances of the stars. The final *Hipparcos* Catalogue was published in June 1997, documenting the parallax, proper motions, radial velocity, right ascension, declination, Galactic coordinates l and b and all associated errors for the stars.

1.4.1 Data Sets

An important point to note is the necessity to analyse the data samples separately. This applies to all studies, where systematic differences in abundances and kinematic data mean it is unreliable to combine data from two or more sources. For this reason, in my results section I have distinguished clearly between the Fulbright sample and the Nissen & Schuster sample. Figure 1.2 gives an idea of where both samples lie with respect to the centre of the Galaxy (note that the graph is not exactly to scale, and rather is used to visualise).

Fulbright Data Set

Fulbright selected 168 stars from multiple sources (for a source list see Fulbright 2000). Fulbright used equivalent widths (EWs) of atomic lines in a self-consistent analysis of the abundances, to produce his sample of high resolution, high signal to noise ratio spectra of mostly metal-poor dwarfs. Local thermodynamic equilibrium (LTE) was assumed, and

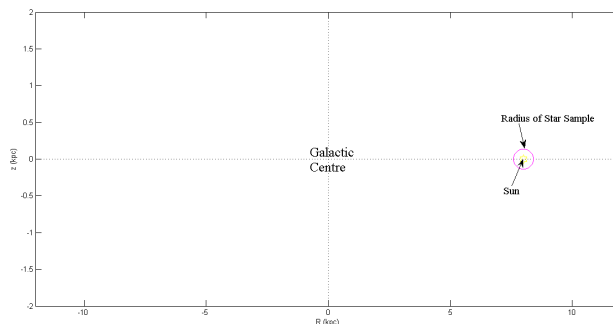


Figure 1.2: Positions of the stellar samples relative to the Galactic Centre. The scale is approximate. The samples probe several hundred pc from the Sun, where the Sun is located at about 8 kpc from the Galactic Center.

line broadening effects from microturbulence (ξ_{turb}) were included. The positions of the Fulbright sample stars relative to the Sun can be seen in Figure 1.3.

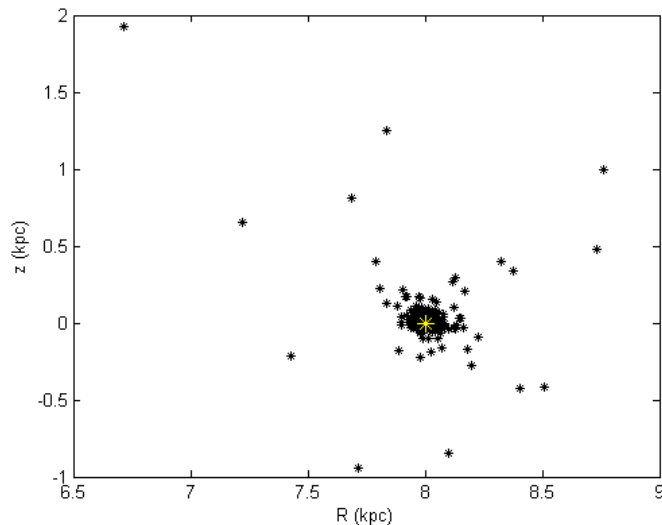


Figure 1.3: Plot of the R and z coordinates of the Fulbright sample of stars relative to the Sun. The Sun is indicated by the larger yellow point.

Nissen and Schuster Data Set

Nissen and Schuster selected their sample from the *uvby- β* catalogue of 100 high-velocity, metal-poor stars. From their catalogue, they selected stars with $-1.6 < [\text{Fe}/\text{H}] < -0.4$. Therefore, their sample is less varied than the Fulbright sample, where Fulbright attempted to select stars with a range of metallicities and abundances. Nissen and Schuster derived precise differential abundance ratios from the equivalent widths (*EWs*) of atomic lines.

They assumed LTE and included line broadening caused by microturbulence (ξ_{turb}) and collisional damping in their abundance analysis. The Nissen & Schuster sample was identified to contain a large number of halo stars and a small number of disk stars. In their paper Nissen & Schuster (2010), it was suggested that the sample contained accreted stars. The positions of their final sample can be seen in Figure 1.4.

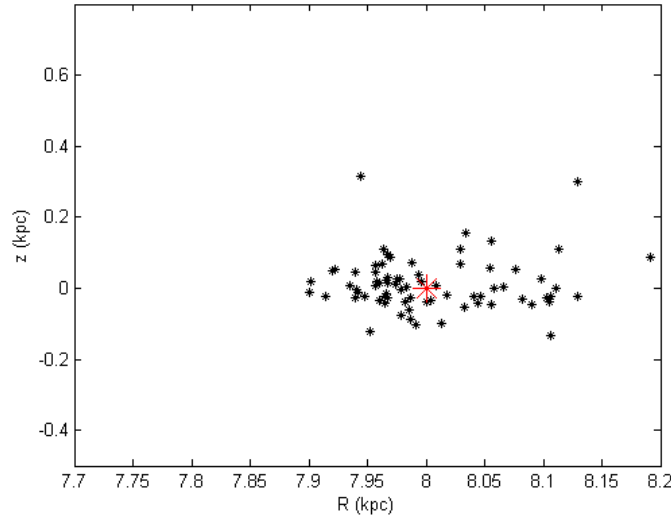


Figure 1.4: Plot of the R and z coordinates of the Nissen & Schuster sample of stars relative to the Sun. The Sun is indicated by the larger red point.

Outline of Method

The first step was to compile all of the chemical and dynamical data in a spreadsheet. This included proper motions, Galactic coordinates, radial velocities and abundances, which were provided by the *Hipparcos* catalogue and selected by Fulbright and Nissen & Schuster. I then calculated the velocities in the Galactic coordinate system: U, V and W using the theory in section 1.2.2. This was computed in Matlab, using the matrix equations provided in Appendix A.

The next step was to compute the energies and angular momenta of the stars. I used a program produced by Greg Ruchti in the language R to carry out the minimisation in equation 1.9. This program output the circular radius value R_c , which I then used to calculate the specific momentum and energy.

Once the data was compiled, I plotted graphs, initially keeping the dynamical and chemical sections separate. For the chemical analysis, I produced abundance plots for several different α elements. I chose magnesium as the predominant element to analyse, in addition to nickel. For the dynamical analysis, I plotted graphs of J_z/J_c against E_z/E_c .

I subsequently combined the chemical and dynamical data to give a full chemodynamical analysis. This was achieved by using Matlab to filter out accreted stars from the sample. In a similar fashion to that in Figure 1.1, I made cuts in the metallicity values of the samples. In each metallicity range, I identified stars with low J_z/J_c and also low $[Mg/Fe]$ and $[Ni/Fe]$ abundance. The graphs providing the chemodynamical analysis are explained in detail in the Results section.

Chapter 2

Results

In this chapter I have included graphs showing the spectral data and the dynamical data of both stellar samples; Fulbright, and Nissen & Schuster. All graphs were plotted in Matlab. The spectral section includes abundance plots as discussed in 1.1.3. The dynamical section includes plots of specific angular momentum and specific energy as discussed in 1.2.4.

Subsequently, I combined the chemical data with the dynamical data of each data set. In this chemodynamical analysis I indicated which stars in each sample are accreted stars.

Therefore, the results will be presented as follows:

- 2.1) Abundance plots for Fulbright and then Nissen & Schuster
- 2.2) J_z/J_c vs E_z/E_c plots for Fulbright and then Nissen & Schuster
- 2.3) Chemodynamical plots for Fulbright and then Nissen & Schuster

Note that the two samples are always plotted separately. This is to avoid systematic errors arising and giving false indications.

2.1 Abundance Plots

2.1.1 Fulbright Data Set

Initially, abundance plots of several alpha and iron group elements were plotted in Matlab. These demonstrate the trends discussed in the theory section. I then chose to present the magnesium graphs as the alpha element, as other alpha elements simply display the same trends, and therefore give no extra information. Magnesium is a good choice of alpha element for this analysis for the following reason. The conclusions drawn are based on the fact that type Ia supernovae produce mainly iron and core-collapse supernovae produce mainly alpha elements. This distinction is what gives us information about the star formation efficiency, based on where the alpha abundance begins to decrease. However, type Ia supernovae also contribute small amounts of the alpha elements, which can make our analysis less clear. According to Tsujimoto et al. (1995), type Ia supernovae contribute less to magnesium abundance than the other alpha elements. This is the reason why magnesium was chosen for this paper.

In addition, I presented the nickel data, as this is an iron group element, and therefore has a different, much flatter, trend to magnesium. The paper by Tolstoy et al. (2009) states that nickel abundances, like magnesium, are lower in dwarf galaxies. If stars show signs of being accreted from both elements, then this provides substantial evidence that they are in fact accreted.

Magnesium

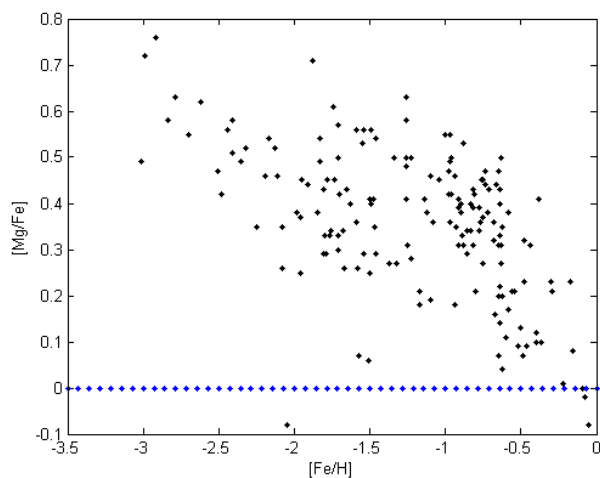


Figure 2.1: Abundance plot of $[\text{Fe}/\text{H}]$ vs $[\text{Mg}/\text{Fe}]$ for the Fulbright star sample. The dotted blue line represents the solar value: $[\text{Mg}/\text{Fe}] = 0$.

Figure 2.1 shows the $[\text{Fe}/\text{H}]$ ratio vs $[\text{Mg}/\text{Fe}]$, like that explained in 1.1.3 and 1.1.5. Around

a metallicity of $[\text{Fe}/\text{H}] \sim -0.5$ there is a visible knee, where alpha abundance drops abruptly. This knee represents where type Ia supernovae began to pollute the interstellar medium from which the stars formed, and the amount of iron present became dominant compared to the abundance of magnesium.

At low metallicity, below $[\text{Fe}/\text{H}] \sim -2$, the $[\text{Mg}/\text{Fe}]$ trend is rather flat, as anticipated. In the intermediate metallicity, up to $[\text{Fe}/\text{H}] \sim -0.8$, there are a range of magnesium abundances. Here, the high $[\text{Mg}/\text{Fe}]$ stars represent the stars formed in situ, where the star formation efficiency is still high. The low $[\text{Mg}/\text{Fe}]$ stars could possibly be accreted stars from a small dwarf galaxy where at these intermediate metallicities the star formation efficiency is lower, and thus the stellar population reached a lower iron abundance (compared to the Milky Way) before type Ia supernovae began to explode. However, the other possibility is that these low $[\text{Mg}/\text{Fe}]$ stars formed in the Milky Way and subsequently migrated radially to the solar neighbourhood from the outer disc, where the star formation efficiency is also lower than the inner disc.

There is also a faint distinction in this intermediate $[\text{Fe}/\text{H}]$ section of the graph, with an upper line and a lower line. This could represent stars from different parts of the Milky Way. However, it is unlikely that this represents the thin and thick disk distinction; it is more likely that the small sample size (167 stars) is the reason why parts of the graph look sparse.

Nickel

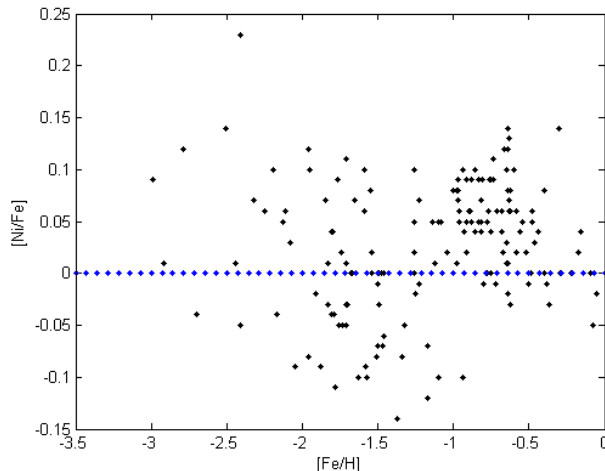


Figure 2.2: Abundance plot of $[\text{Fe}/\text{H}]$ vs $[\text{Ni}/\text{Fe}]$ for the Fulbright star sample. The dotted blue line represents the solar value: $[\text{Ni}/\text{Fe}] = 0$.

Nickel abundances tend to lie close to the solar value, as demonstrated by Figure 2.2. Sim-

ilar to the magnesium abundance, at metallicities below ~ -0.8 , there is a group of stars with low $[\text{Ni}/\text{Fe}]$ ratios. These could possibly be accreted stars, or they could be halo stars.

There were similar trends in both magnesium and nickel abundances, with some stars displaying low $[\text{Mg}/\text{Fe}]$ and $[\text{Ni}/\text{Fe}]$ values at lower metallicity values. This is promising in the search for accreted stars. However, to indicate whether the stars with low $[\text{Mg}/\text{Fe}]$ also had low $[\text{Ni}/\text{Fe}]$, a graph of the magnesium-nickel relation was plotted. Although the graph

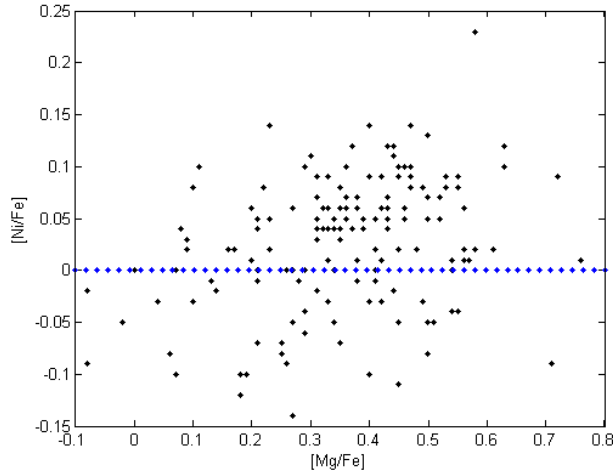


Figure 2.3: $[\text{Mg}/\text{Fe}]$ vs $[\text{Ni}/\text{Fe}]$ for the Fulbright data. The dotted blue line represents the solar value: $[\text{Ni}/\text{Fe}] = 0$.

appears scattered, there is an overall trend, if somewhat vague, that some stars with lower $[\text{Mg}/\text{Fe}]$ also display low $[\text{Ni}/\text{Fe}]$. These stars are the most likely to have been accreted.

2.1.2 Nissen and Schuster Data Set

Magnesium

Figure 2.4 shows that the range of $[\text{Mg}/\text{Fe}]$ and $[\text{Fe}/\text{H}]$ values for the Nissen & Schuster data set is narrower than for the Fulbright data. This is due to their selection techniques. At metallicities $-1.6 < [\text{Fe}/\text{H}] < -0.8$, there is a group of high $[\text{Mg}/\text{Fe}]$ abundance stars, corresponding to in situ disc stars. There is also a group of low $[\text{Mg}/\text{Fe}]$ stars which could be accreted.

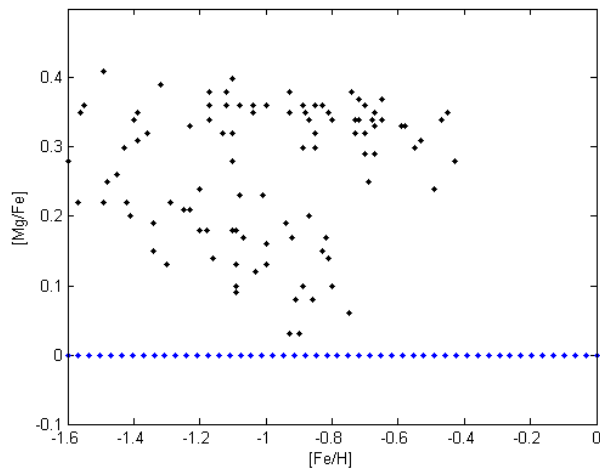


Figure 2.4: Abundance plot of $[\text{Fe}/\text{H}]$ vs $[\text{Mg}/\text{Fe}]$ for the Nissen & Schuster star sample. The dotted blue line represents the solar value: $[\text{Mg}/\text{Fe}] = 0$.

Nickel

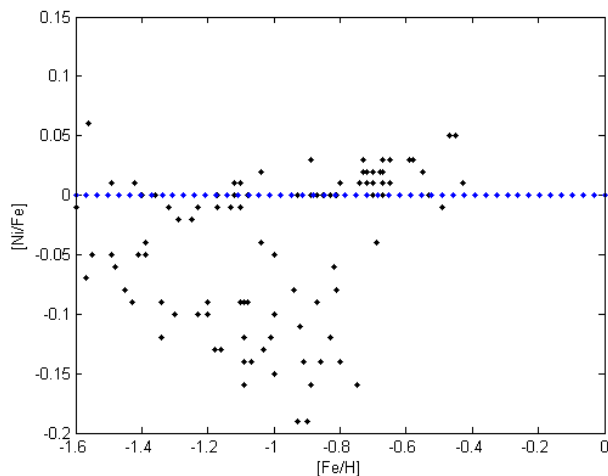


Figure 2.5: Abundance plot of $[\text{Fe}/\text{H}]$ vs $[\text{Ni}/\text{Fe}]$ for the Nissen & Schuster star sample. The dotted blue line represents the solar value: $[\text{Ni}/\text{Fe}] = 0$.

Figure 2.5 shows the nickel abundance for the Nissen & Schuster data. The general trend is flat, with most stars lying within 0.1 of the solar nickel abundance. There are many stars with $[\text{Fe}/\text{H}]$ below ~ -0.8 which lie below the $[\text{Ni}/\text{Fe}] = 0$ line. Once again, there appears to be a clear distinction between the upper and lower line, which at first look appears to indicate stars with two distinct origins. However, due to small number statistics, it is unlikely that the case is this simple. Further analysis of the low nickel abundance stars is

required to indicate which of these are accreted stars.

At low metallicities, there were stars with both low magnesium and nickel abundances. A graph of $[\text{Mg}/\text{Fe}]$ vs $[\text{Ni}/\text{Fe}]$ was plotted in Figure 2.6 to determine whether the stars with low magnesium abundance also had low nickel abundance. Figure 2.6 shows a far

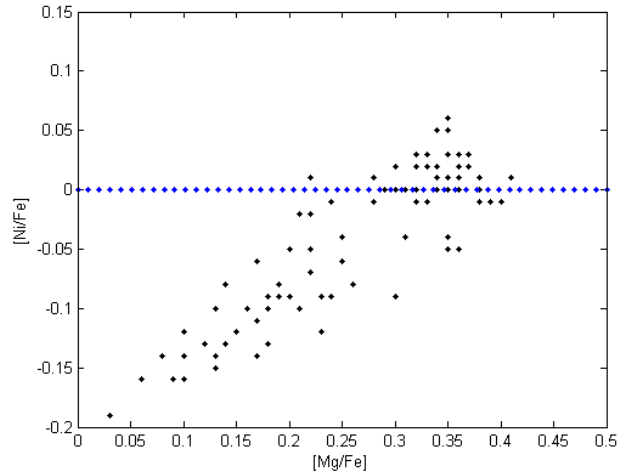


Figure 2.6: $[\text{Mg}/\text{Fe}]$ vs $[\text{Ni}/\text{Fe}]$ for the Nissen & Schuster data. The dotted blue line represents the solar value: $[\text{Ni}/\text{Fe}] = 0$.

clearer correlation between $[\text{Mg}/\text{Fe}]$ and $[\text{Ni}/\text{Fe}]$ than that found for the Fulbright data set. This means that there were a significant number of stars with uncharacteristically low magnesium and nickel abundances, which therefore give promising evidence for accreted stars in the Nissen & Schuster sample. Further analysis of the dynamics of the data uncovers more information about accreted stars in the sample.

2.2 Orbits Plots

2.2.1 Fulbright Data Set

The plot in Figure 2.7 gives an insight into the orbits of the Fulbright stellar sample. There is a tight cluster in the top right corner, meaning specific angular momentum and specific energy in the z-direction are near one. As discussed in 1.2.4, these stars are on near-circular orbits. One can therefore conclude that these stars formed inside the Milky Way and retained their circular orbit due to momentum conservation. However, from this graph alone it is not possible to tell if they were formed where they are today (in close proximity to the Sun) or if they formed elsewhere and radially migrated, as discussed in 1.3.2. This would require knowledge of the ages and abundances of the stars, and can be resolved in the chemodynamical section.

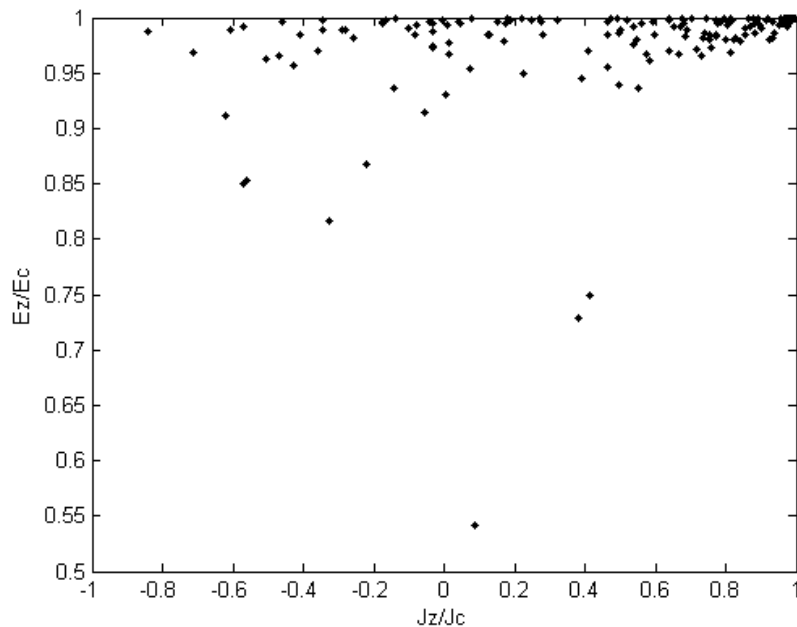


Figure 2.7: Graph of J_z/J_c against E_z/E_c for the Fulbright data set. A value of $J_z/J_c = E_z/E_c = 1$ indicates a circular, in plane orbit.

There are many stars in the sample which have lower J_z/J_c values, below ~ 0.6 . There are even some with negative specific angular momenta, meaning they are moving on retrograde rather than prograde orbits. This opens up the question whether these stars have been accreted. However, these stars could also be halo stars, which move on characteristically non-circular orbits. Again, further analysis in the chemodynamical section will shed more light on this.

2.2.2 Nissen and Schuster Data Set

From Figure 2.8, it is clear that there are far fewer stars with specific angular momentum and specific energy of near one in the Nissen & Schuster data. This implies that this sample of stars consists of fewer in situ stars and many have been accreted. This further backs up the outcome of the chemical analysis, which also indicated that the Nissen & Schuster sample contained accreted stars.

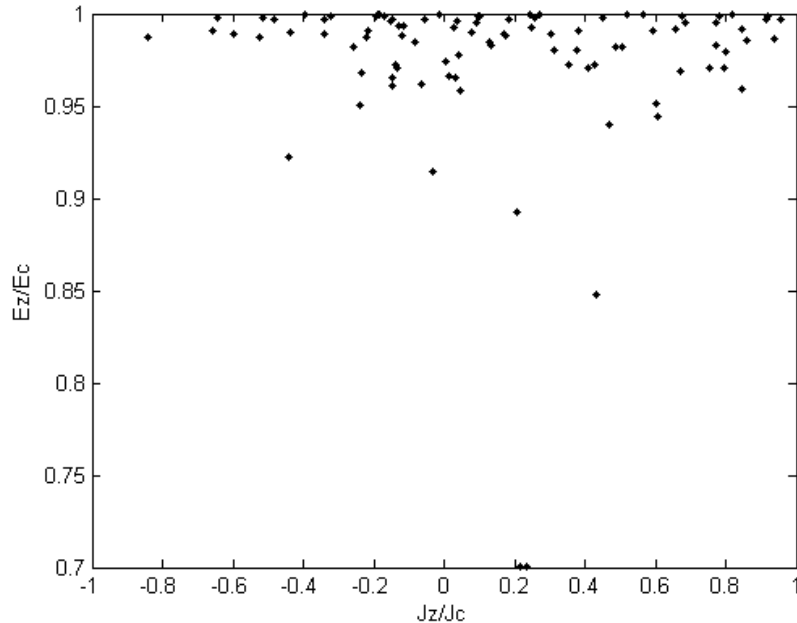


Figure 2.8: Graph of J_z/J_c against E_z/E_c for the Nissen & Schuster data set. A value of $J_z/J_c = E_z/E_c = 1$ indicates a circular, in plane orbit.

2.3 Chemodynamical Analysis

In this section, I combined the dynamical and chemical data to draw my conclusions about the substructure in the Milky Way. This included finding accreted stars and distinguishing them from stars which have migrated through the Galaxy.

Initially, I analysed magnesium, as my abundance plots showed potential for accreted stars. In addition to this, I continued my analysis of nickel, an iron-peak element. These two elements are produced in different ways in supernovae, and therefore finding low abundances of both is a good indicator for accreted stars. I also carried out the analysis of other α elements, but these followed the same trends as magnesium, and gave no further insight into finding accreted stars.

In order to distinguish the accreted stars from the in situ stars, I cut the data based on the metallicities and α abundances. The cuts I made are based on the results from Ruchti et al. (2014). The study used several simulated merger events of satellite galaxies with the Milky Way and observed the specific angular momenta and energies of in situ and accreted stars after the merger. The study focussed on magnesium as the α element and found that accreted stars have $[Mg/Fe] < 0.3$ and $J_z/J_c < 0.8$.

2.3.1 Fulbright Data Set

Magnesium

The first α element I analysed was magnesium. I cut the metallicity at three points; high-metallicity $[\text{Fe}/\text{H}] > -0.8$, intermediate metallicity $-1.3 < [\text{Fe}/\text{H}] < -0.8$, and finally low metallicity $[\text{Fe}/\text{H}] < -1.3$. In these three bins, I then defined the high $[\text{Mg}/\text{Fe}]$ abundance as greater than 0.3 based on the aforementioned study Ruchti et al. (2014) and compared it to the low $[\text{Mg}/\text{Fe}]$ abundance defined as lower than 0.3. These cuts are best visualised on the magnesium abundance plot, shown in Figure 2.9.

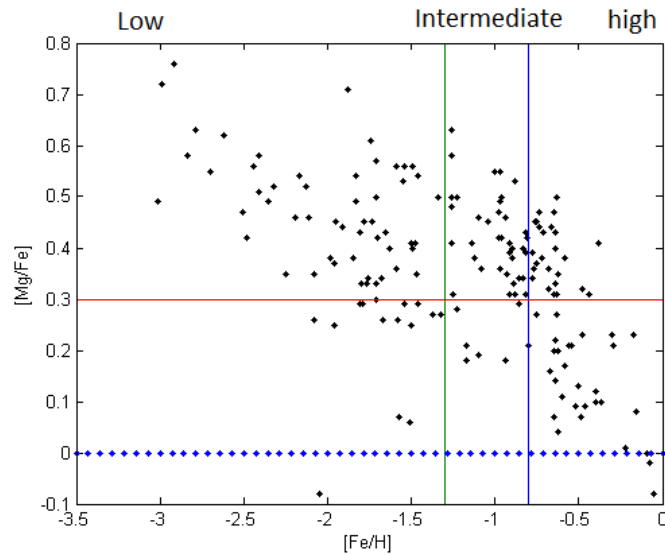


Figure 2.9: $[\text{Mg}/\text{Fe}]$ as a function of $[\text{Fe}/\text{H}]$, demonstrating the metallicity and abundance cuts in the Fulbright data.

After separating the data into these bins, I then analysed the specific angular momenta of the stars. For each metallicity bin, I plotted the specific angular momentum against specific energy, using different colours to differentiate between low and high α abundances. Next, instead of just using the data points as they were, I incorporated the uncertainties by first computing a normal distribution for each star, centred on its J_z/J_c value. This provided a probability distribution of angular momentum for each star. I then summed the J_z/J_c distributions for all stars within a given metallicity bin to determine the overall J_z/J_c distribution in that bin.

Figures 2.10 A1 and A2 show data for the lowest metallicity stars, $[\text{Fe}/\text{H}] < -1.3$. The blue stars give the probability distribution for high $[\text{Mg}/\text{Fe}]$ abundances and the red stars for low $[\text{Mg}/\text{Fe}]$ abundances. In Figure 2.10 A2, there is a peak at $J_z/J_c \sim 0.8$ for high $[\text{Mg}/\text{Fe}]$. This corresponds to the in situ stars moving on relatively circular orbits.

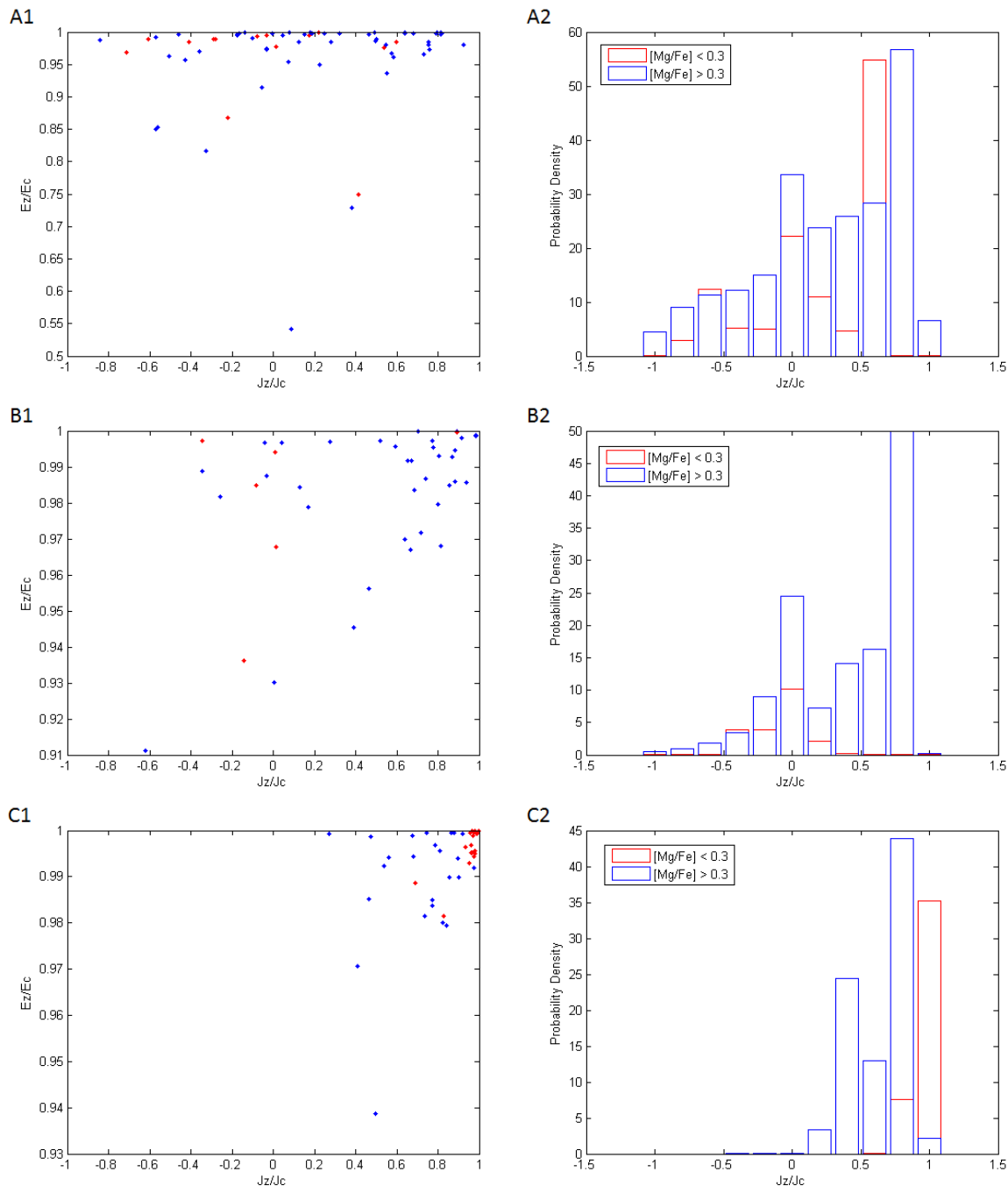


Figure 2.10: Graphs A1, B1 and C1 show J_z/J_c against E_z/E_c for the Fulbright data set, with low $[Mg/Fe]$ plotted in red and high $[Mg/Fe]$ plotted in blue. Graphs A2, B2 and C2 show the probability distribution in J_z/J_c for the Fulbright data set, with low $[Mg/Fe]$ plotted in red and high $[Mg/Fe]$ plotted in blue. A1 and A2 show the data for metallicity bin $[Fe/H] < -1.3$. B1 and B2 show the data for metallicity bin $-1.3 < [Fe/H] < -0.8$. C1 and C2 show the data for metallicity bin $[Fe/H] > -0.8$.

In Figure 2.10 A2, there is also a peak at $J_z/J_c \sim 0.6$ in the low $[\text{Mg}/\text{Fe}]$ stars moving on high J_z/J_c orbits. These are unlikely to be accreted dwarf galaxy stars due to their low eccentricity. One possible explanation could be that these stars came from an earlier merger with a massive galaxy, where the stars are deposited on more prograde orbits. However, this is unlikely, as the alpha abundances for a massive accretion event would then be higher. Furthermore, the study Ruchti et al. (2015) searched for evidence of massive accretion events and found none. Therefore, the most likely explanation is that these are in situ disk stars, whose $[\text{Mg}/\text{Fe}]$ abundances lie at the low alpha tail of the disk.

Figure 2.10 A2 also shows a distribution of low $[\text{Mg}/\text{Fe}]$ stars at lower J_z/J_c values, centred on zero. They are therefore stars which likely formed in a dwarf spheroidal galaxy outside the Milky Way, where the alpha abundances are lower due to lower star formation efficiency. The fact that they are moving on clear non-circular orbits reinforces this. There are 14 stars with $[\text{Mg}/\text{Fe}] < 0.3$ and $J_z/J_c < 0.8$, which have been identified as accreted stars, out of a total sample size of 167 stars.

There is also a peak in high $[\text{Mg}/\text{Fe}]$ abundances on non-circular orbits. These are less likely to be accreted stars because their $[\text{Mg}/\text{Fe}]$ abundance indicates they originated in an environment with a higher star formation efficiency than a small satellite galaxy would have. However, there is another explanation for these stars. It is very possible these are halo stars. Some astronomers believe that the Milky Way halo formed from early accretion events of more massive dwarf galaxies which had higher α and iron group element abundances than present day satellite galaxies. See (e.g. Font et al. 2011) for a cosmological hydrodynamical simulation of the formation of stellar haloes. Halo stars have a tendency to be on less circular orbits than the disk stars. Therefore, the high $[\text{Mg}/\text{Fe}]$ stars most likely correspond to halo stars.

Figures 2.10 B1 and B2 show the data for the stars with $-1.3 < [\text{Fe}/\text{H}] < -0.8$. The axis in Figure 2.10 B2 has been cut due to a peak at high angular momentum where the error was extremely low. There is a peak at high angular momentum in the distribution for the high $[\text{Mg}/\text{Fe}]$ stars. These correspond to in situ Milky Way stars.

There are also high $[\text{Mg}/\text{Fe}]$ stars at low J_z/J_c values centred on zero, including stars on retrograde orbits. Again, these are likely to be halo stars on radical orbits.

The low $[\text{Mg}/\text{Fe}]$ abundance stars lie predominantly at low angular momenta, meaning they have been accreted from small satellite galaxies. There are a total of 5 stars in this intermediate metallicity range which are accreted.

Figures 2.10 C1 and C2 show the stars with $[\text{Fe}/\text{H}] > -0.8$. The theory outlined previously dictates that small satellite galaxies don't reach such high metallicity values, because their star formation efficiency isn't sufficiently high. Therefore, the consensus should be that most of these stars are in situ. Figure 2.10 C2 confirms this. The red stars are low magne-

sium abundance stars predominantly on circular orbits. As they have low $[\text{Mg}/\text{Fe}]$, without the dynamical analysis, one might incorrectly assume that they were accreted. However, as they are on circular orbits, it is more likely that these are thin disc stars moving on circular orbits.

The high $[\text{Mg}/\text{Fe}]$ stars on non-circular orbits are probably heated disc stars in the high eccentricity orbits tail of the thick disc. They could also be associated with the high $[\text{Mg}/\text{Fe}]$ tail of the halo stars.

Figure 2.10 C1 shows that there are very few stars with J_z/J_c near or below 0, confirming that at high metallicity very few or no stars show evidence of accretion. In the low $[\text{Mg}/\text{Fe}]$ range, there is only 1 star from the entire sample which lies at $J_z/J_c < 0.8$, demonstrating the restrictions of low number statistics.

Nickel

When analysing the nickel abundance of the Fulbright data, I chose the low $[\text{Ni}/\text{Fe}]$ value to be 0, as nickel abundance is typically lower in the Milky Way (e.g. Soubiran & Girard 2005). I kept the cuts in metallicity the same as for magnesium. The cuts in metallicity and $[\text{Ni}/\text{Fe}]$ are shown in Figure 2.11.

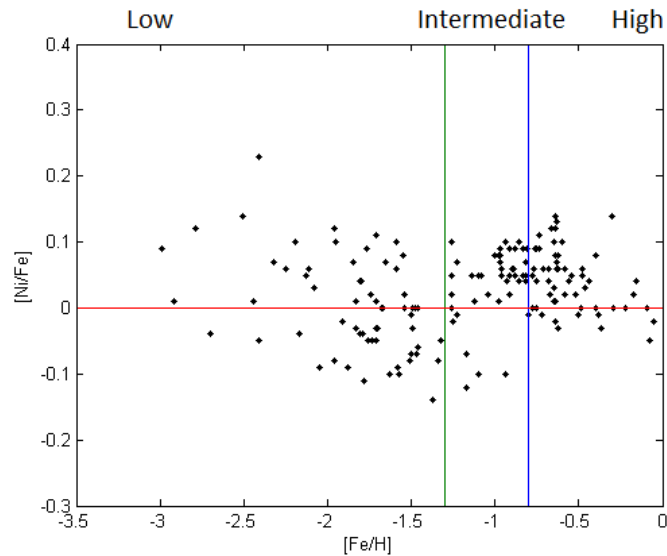


Figure 2.11: $[\text{Ni}/\text{Fe}]$ as a function of $[\text{Fe}/\text{H}]$, demonstrating the metallicity and abundance cuts in the Fulbright data

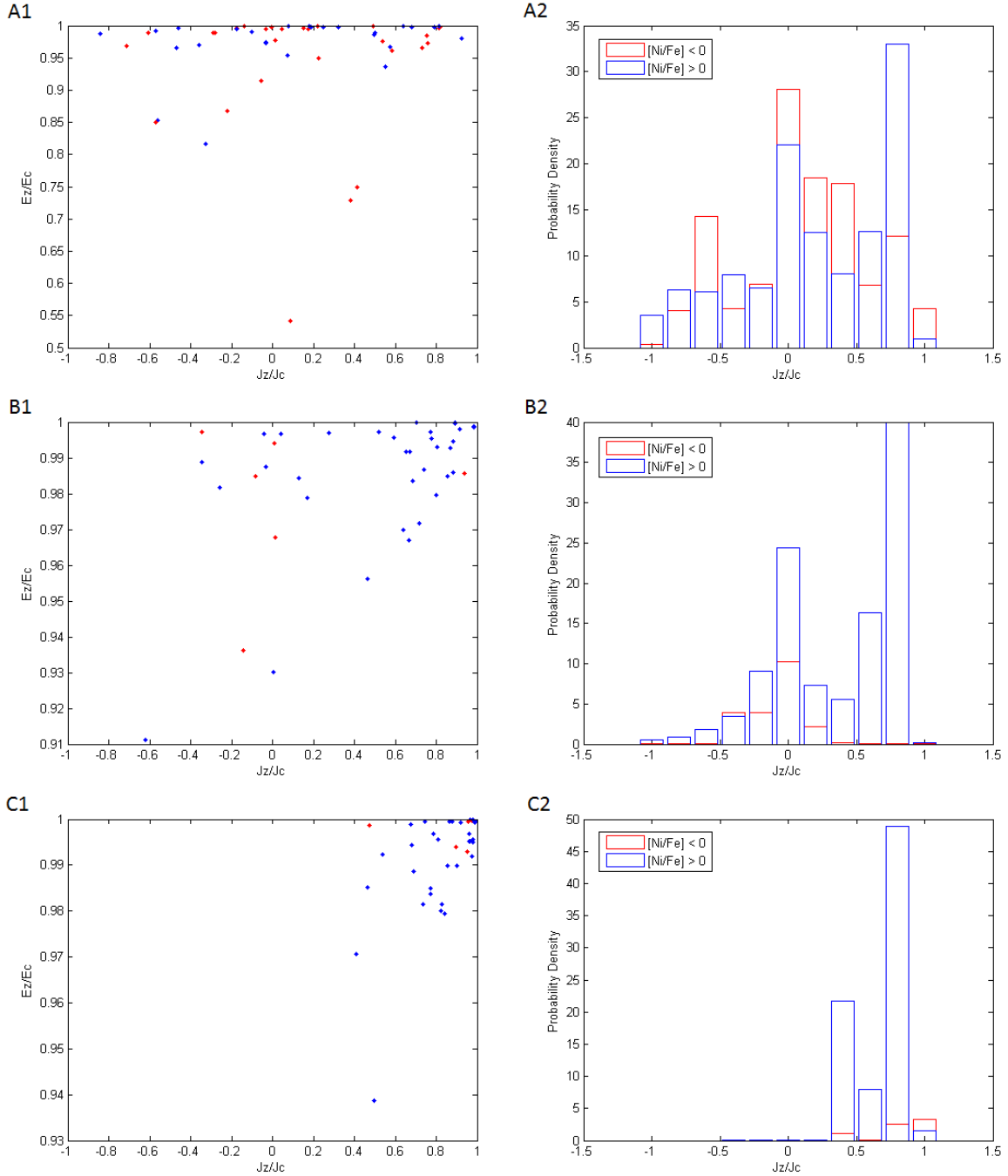


Figure 2.12: Graphs A1, B1 and C1 show J_z/J_c against E_z/E_c for the Fulbright data set, with low $[Ni/Fe]$ plotted in red and high $[Ni/Fe]$ plotted in blue. Graphs A2, B2 and C2 show the probability distribution in J_z/J_c for the Fulbright data set, with low $[Ni/Fe]$ plotted in red and high $[Ni/Fe]$ plotted in blue. A1 and A2 show the data for metallicity bin $[Fe/H] < -1.3$. B1 and B2 show the data for metallicity bin $-1.3 < [Fe/H] < -0.8$. C1 and C2 show the data for metallicity bin $[Fe/H] > -0.8$.

Figures 2.12 A1 and A2 show the Fulbright stars with the lowest metallicity, $[\text{Fe}/\text{H}] < -1.3$. A2 shows there are some stars with high nickel abundance on near circular orbits with $J_z/J_c \sim 0.8$, which correspond to the in situ Milky Way stars. Many stars are moving on non-circular and even retrograde orbits. Those with low nickel abundance are most likely accreted stars. There appear to be more accreted stars from a $[\text{Ni}/\text{Fe}]$ analysis than for $[\text{Mg}/\text{Fe}]$. In this low metallicity range, there were 26 stars with low $[\text{Ni}/\text{Fe}]$ and J_z/J_c . This could be due to my choice of distinction between low and high $[\text{Ni}/\text{Fe}]$ at 0. However, the presence of accreted stars backs up the results from the $[\text{Mg}/\text{Fe}]$ analysis.

The stars with high nickel abundance on non-circular orbits are most likely halo-like stars, for the same reasons outlined in the magnesium analysis.

Figures 2.12 B1 and B2 show the specific angular momentum for stars in the metallicity range $-1.3 < [\text{Fe}/\text{H}] < -0.8$. In this intermediate metallicity bin, nickel displays the same trends as magnesium. The tall peak in high $[\text{Ni}/\text{Fe}]$ abundance on circular orbits corresponds to in situ stars. The peaks in high $[\text{Ni}/\text{Fe}]$ abundance on non-circular and retrograde orbits correspond to halo stars moving on radical orbits.

The accreted stars are showed by the low $[\text{Ni}/\text{Fe}]$ abundance stars with J_z/J_c centred around 0. Figure 2.15 B1 shows evidence of 5 stars with these properties, the same number that was indicated from the $[\text{Mg}/\text{Fe}]$ analysis in this metallicity range. This gives more confidence that these stars are accreted.

Figures 2.12 C1 and C2 show the stars with the highest metallicity of $[\text{Fe}/\text{H}] > -0.8$. The graphs show that the stars are predominantly in situ. Most of the stars move on circular orbits with $J_z/J_c \sim 0.8$, and exhibit high $[\text{Ni}/\text{Fe}]$ abundances. There is only a single star which has low $[\text{Ni}/\text{Fe}]$ and moves on a non-circular orbit, which was the same result found from the $[\text{Mg}/\text{Fe}]$ analysis.

In the Fulbright data set, the stars indicated as accreted from the $[\text{Mg}/\text{Fe}]$ abundance plots were cross-referenced with the accreted stars from the $[\text{Ni}/\text{Fe}]$ abundance plots. The stars which appeared to be accreted from analysis in both elements are the stars which I can state with confidence are accreted. There are a total of 18 stars in the Fulbright data set which are accreted.

2.3.2 Nissen and Schuster Data Set

I carried out the same chemodynamical analysis on the Nissen & Schuster set of stars.

Magnesium

Similarly to the Fulbright data set, I made cuts in the metallicity and $[\text{Mg}/\text{Fe}]$ abundances. For magnesium I used the same values as for the Fulbright data to section the data.

Beginning with magnesium, these cuts can be visualised from the graph in Figure 2.13.

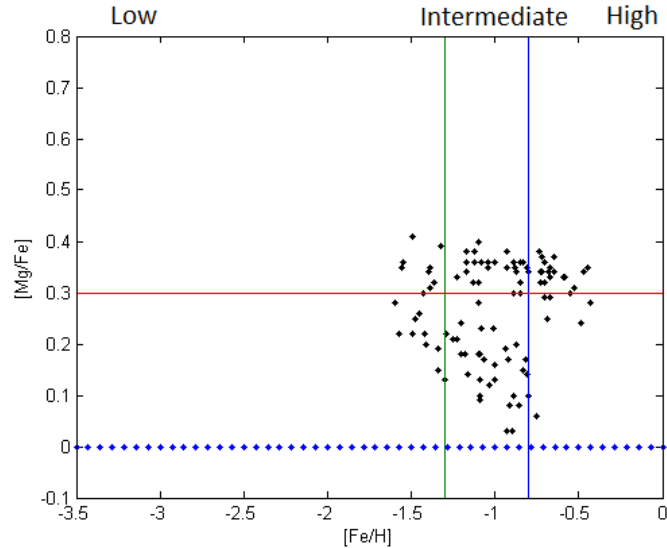


Figure 2.13: $[\text{Mg}/\text{Fe}]$ as a function of $[\text{Fe}/\text{H}]$, demonstrating the metallicity and abundance cuts in the Nissen & Schuster data

Figures 2.14 A1 and A2 show the stars with $[\text{Fe}/\text{H}] < -1.3$. In contrast to the Fulbright sample, all but one of the stars are moving on non-circular orbits, with J_z/J_c values centred on zero. The stars with high $[\text{Mg}/\text{Fe}]$ values are likely halo stars, because their orbits are too radical to be associated with the thick disk. The accreted stars are those with low $[\text{Mg}/\text{Fe}]$ abundances. There are 8 stars in this low metallicity range which appear to be accreted, out of a total of 100 in the entire data set.

Figures 2.14 B1 and B2 show the stars with $-1.3 < [\text{Fe}/\text{H}] < -0.8$. In this intermediate metallicity range, the in situ stars are clearly seen in the peak of high $[\text{Mg}/\text{Fe}]$ on near circular orbits, with $J_z/J_c \sim 0.8$. The high $[\text{Mg}/\text{Fe}]$ peak at a J_z/J_c of 0 are halo stars, as expected.

The two large peaks in low $[\text{Mg}/\text{Fe}]$ abundance stars moving on retrograde orbits correspond to accreted stars. There are 27 stars in this metallicity range which show clear signs of accretion.

Figures 2.14 C1 and C2 show the stars with the highest metallicity of $[\text{Fe}/\text{H}] > -0.8$. The probability density graph in C2 shows that most stars have high $[\text{Mg}/\text{Fe}]$ abundances, suggesting the presence of predominantly in situ disk stars and halo stars. C1 shows that there are 5 stars with low $[\text{Mg}/\text{Fe}]$ abundance moving on low J_z/J_c orbits. It is unlikely that these stars are accreted, because stars from a dwarf galaxy wouldn't have such high $[\text{Fe}/\text{H}]$ ratios. Therefore, these are most likely the low $[\text{Mg}/\text{Fe}]$ tail of the halo.

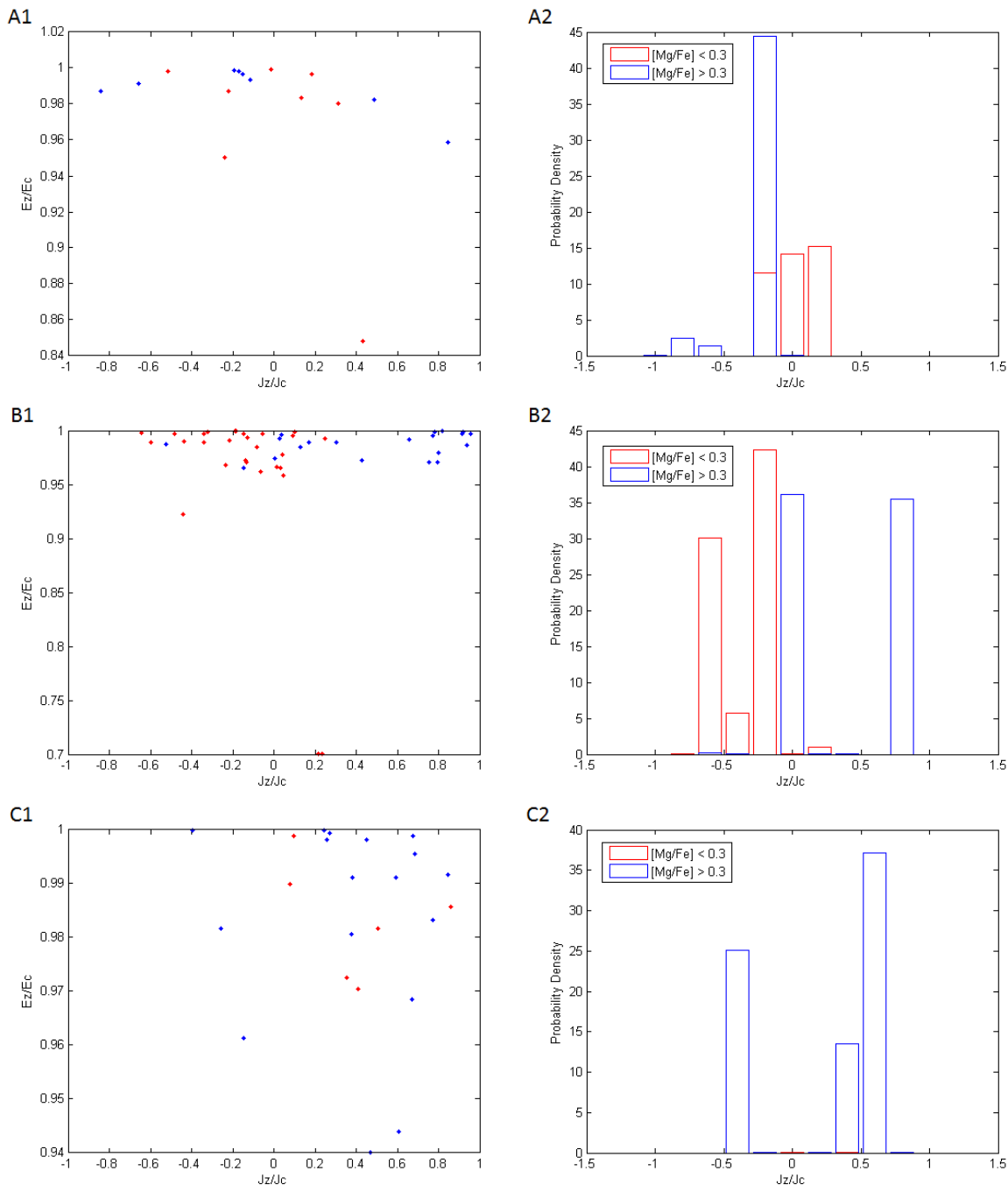


Figure 2.14: Graphs A1, B1 and C1 show J_z/J_c against E_z/E_c for the Nissen & Schuster data set, with low $[\text{Mg}/\text{Fe}]$ plotted in red and high $[\text{Mg}/\text{Fe}]$ plotted in blue. Graphs A2, B2 and C2 show the probability distribution in J_z/J_c for the Nissen & Schuster data set, with low $[\text{Mg}/\text{Fe}]$ plotted in red and high $[\text{Mg}/\text{Fe}]$ plotted in blue. A1 and A2 show the data for metallicity bin $[\text{Fe}/\text{H}] < -1.3$. B1 and B2 show the data for metallicity bin $-1.3 < [\text{Fe}/\text{H}] < -0.8$. C1 and C2 show the data for metallicity bin $[\text{Fe}/\text{H}] > -0.8$.

Nickel

For the Nissen & Schuster stellar sample, there was a divide in nickel abundances at $[\text{Ni}/\text{Fe}] = -0.05$. As the general trend of nickel abundance was lower than for the Fulbright sample, I chose to define the low $[\text{Ni}/\text{Fe}]$ as stars with $[\text{Ni}/\text{Fe}]$ below -0.05 . This cut can be seen on Figure 2.15.

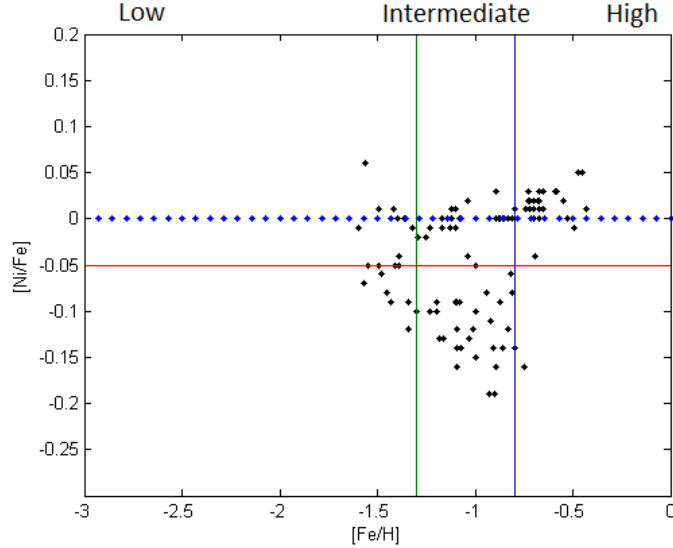


Figure 2.15: $[\text{Ni}/\text{Fe}]$ as a function of $[\text{Fe}/\text{H}]$, demonstrating the metallicity and abundance cuts in the Nissen & Schuster data

The stars with the lowest metallicities, $[\text{Fe}/\text{H}] < -1.3$, are shown in Figures 2.16 A1 and A2. There are few stars with both high J_z/J_c values and high $[\text{Ni}/\text{Fe}]$ values, meaning there are few in situ disk stars. There are stars moving on retrograde orbits, with negative J_z/J_c , which have high $[\text{Ni}/\text{Fe}]$ abundance. These are halo stars. A number of the stars with $[\text{Fe}/\text{H}] < -1.3$ are moving on non-circular orbits with low $[\text{Ni}/\text{Fe}]$ abundances, and are therefore evidence of accretion. There are 6 stars from the entire sample in this metallicity range which are accreted. This is a similar number to the results found from analysing $[\text{Mg}/\text{Fe}]$ at low metallicity. This gives further evidence that there are accreted stars in this sample.

Figures 2.16 B1 and B2 show the stars with $-1.3 < [\text{Fe}/\text{H}] < -0.8$. The in situ disk stars appear here as the high $[\text{Ni}/\text{Fe}]$ abundance stars moving on circular orbits with a peak at $J_z/J_c \sim 0.7$. The stars moving on non-circular orbits with high $[\text{Ni}/\text{Fe}]$ abundance are halo stars. There are stars moving on retrograde orbits with low nickel abundance, which are the accreted stars. There are 24 accreted stars in this metallicity range. This is a similar number to those which also had low $[\text{Mg}/\text{Fe}]$ abundance.

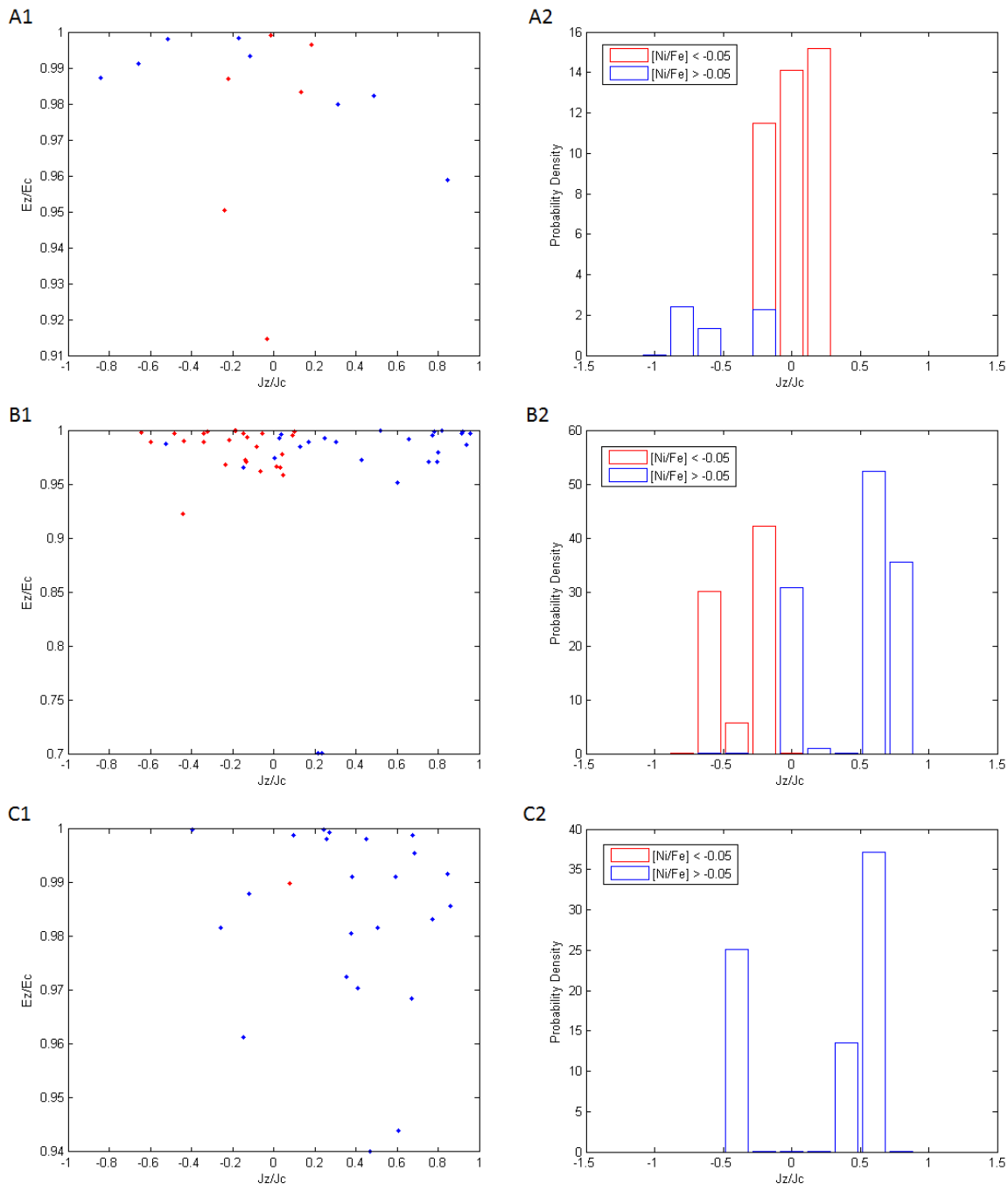


Figure 2.16: Graphs A1, B1 and C1 show J_z/J_c against E_z/E_c for the Nissen & Schuster data set, with low $[\text{Ni}/\text{Fe}]$ plotted in red and high $[\text{Ni}/\text{Fe}]$ plotted in blue. Graphs A2, B2 and C2 show the probability distribution in J_z/J_c for the Nissen & Schuster data set, with low $[\text{Ni}/\text{Fe}]$ plotted in red and high $[\text{Ni}/\text{Fe}]$ plotted in blue. A1 and A2 show the data for metallicity bin $[\text{Fe}/\text{H}] < -1.3$. B1 and B2 show the data for metallicity bin $-1.3 < [\text{Fe}/\text{H}] < -0.8$. C1 and C2 show the data for metallicity bin $[\text{Fe}/\text{H}] > -0.8$.

Figures 2.16 C1 and C2 show the stars with $[\text{Fe}/\text{H}] > -0.8$. In this metallicity range there are disk stars with high $[\text{Ni}/\text{Fe}]$ which lie in the low angular momentum tail of the disk, with $J_z/J_c \sim 0.6$. The stars with high $[\text{Ni}/\text{Fe}]$ and $J_z/J_c \sim -0.4$ are halo stars. C1 shows that there is only 1 star which could possibly be accreted, and due to small number statistics, this is not sufficient evidence of accretion.

In the Nissen & Schuster sample of data, there were a total of 29 stars which had $J_z/J_c < 0.8$ in addition to low values of both $[\text{Mg}/\text{Fe}]$ and $[\text{Ni}/\text{Fe}]$. Therefore, there is sufficient evidence to identify these 29 stars as accreted.

Chapter 3

Conclusion

In this thesis, I analysed the data from two sets of stars; Fulbright and Nissen & Schuster. The goal was to identify stars in each sample which had been accreted from dwarf galaxies. This required an understanding of the theory necessary to apply a chemodynamical analysis to a stellar sample.

Initially, I carried out a chemical analysis of the abundances of $[\text{Mg}/\text{Fe}]$ and $[\text{Ni}/\text{Fe}]$ vs $[\text{Fe}/\text{H}]$. From this analysis, I indicated which stars in each sample could be accreted stars. My abundance plots for $[\text{Mg}/\text{Fe}]$ vs $[\text{Fe}/\text{H}]$ agreed with other research in magnesium, (e.g. Ruchti et al. 2014; Tolstoy et al. 2009). The analysis of nickel confirmed the conclusion that both samples contained accreted stars. Furthermore, fewer studies have been carried out on $[\text{Ni}/\text{Fe}]$ vs $[\text{Fe}/\text{H}]$, and this therefore opens up the possibility of identifying accretion from nickel abundances.

Following on from the chemical analysis, I carried out a dynamical analysis on the data by plotting J_z/J_c vs E_z/E_c for each data set. From these graphs, I identified the stars at low specific angular momentum and specific energy as stars which showed signs of being accreted. However, at this point it was not possible to say with certainty that the stars were accreted.

In the final section, I split the metallicity of the stars into three bins; low, intermediate and high. In each bin, I distinguished between low and high $[\text{Mg}/\text{Fe}]$ or $[\text{Ni}/\text{Fe}]$ values. I made an additional distinction between low and high specific angular momenta values. By making these cuts in the data, I successfully identified 18 accreted stars from the Fulbright sample and 29 accreted stars from the Nissen & Schuster sample. This method helped me to identify the accreted stars with more confidence than if only a chemical or dynamical analysis had been used. In the chemodynamical analysis, I incorporated the uncertainties in J_z/J_c by plotting the specific angular momentum as a probability density graph. These uncertainties are determined by the uncertainty in parallax, proper motion and radial velocity, as outlined in Appendix A. After incorporating the uncertainties in the dynamical data, the two samples continued to show evidence of accreted stars, which

increases the confidence in the results.

With my chemodynamical analysis, I found evidence of accreted stars from small merger events. These were defined by their low J_z/J_c values and low $[\text{Mg}/\text{Fe}]$ and $[\text{Ni}/\text{Fe}]$ abundances, appearing at low $[\text{Fe}/\text{H}]$. There was no evidence of accreted stars from a massive merger. These stars would appear at higher $[\text{Fe}/\text{H}]$ values, and their J_z/J_c values would be slightly higher, on prograde orbits. This puts a constraint on the merger history of the Milky Way, as it implies that there have been no major mergers since the Galactic disk formed.

The main disadvantage to this study results from low number statistics. For sample sizes of 100 and 167, there is a risk of drawing false conclusions. In addition, the small sample sizes mean that this study isn't representative of the entire galaxy. However, the aim was to gain knowledge about the merger history of the Galaxy by identifying accreted stars. The fact that there were accreted stars in both samples means that the Milky Way has experienced merger events with small dwarf galaxies in the past, and therefore meets the aim of this study.

Furthermore, biases in the sample restrict the variety of stars available to analyse. Nissen and Schuster had previously suggested that their sample contained accreted stars, and therefore my chemodynamical analysis of their data identified a large fraction of the stars as accreted. Fulbright attempted to reduce selection biases by selecting stars from a range of sources. However, these sources themselves will contain some biases.

Despite this, the aim of the thesis was met, as I was able to successfully identify accreted stars which form substructure in the Milky Way.

To overcome the disadvantage of small data samples, a much larger, unbiased sample is necessary. In several years, this will become possible, due to new surveys such as the *Gaia* survey, which will take data from many thousands of stars in the Milky Way.

If given more time, and a larger sample, I would have carried out an in depth search for accreted stars. In particular, it would be interesting to look for stars which were accreted from a common source based on their abundances and orbits. Furthermore, these stars could then be related to the dwarf galaxy which they were accreted from.

In future work I would also explore further the analysis of $[\text{Ni}/\text{Fe}]$ ratios in the Milky Way. In contrast to $[\text{Mg}/\text{Fe}]$ ratios which have been studied extensively, nickel is an uncommon element to analyse. As this is a new concept, there is potential to uncover new knowledge about accreted stars based on their $[\text{Ni}/\text{Fe}]$ ratios.

Astronomers look for accreted stars in the Milky Way because it constrains the merger history of the Milky Way. This gives insight into how the Galaxy has evolved over time.

When the Milky Way is understood, the knowledge can be applied to other galaxies to understand how they have formed and evolved over time. Constraining the merger history of the Milky Way is the first stepping stone in uncovering the theory behind Galactic evolution.

Bibliography

- Bensby, T., Feltzing, S., & Oey, M. S. 2014, *A&A*, 562, A71
- Bovy, J., Rix, H.-W., & Hogg, D. W. 2012, *ApJ*, 751, 131
- Eyer, L., Dubath, P., Saesen, S., et al. 2012, in *IAU Symposium*, Vol. 285, *IAU Symposium*, ed. E. Griffin, R. Hanisch, & R. Seaman, 153–157
- Font, A. S., McCarthy, I. G., Crain, R. A., et al. 2011, *MNRAS*, 416, 2802
- Freeman, K. & Bland-Hawthorn, J. 2002, *ARA&A*, 40, 487
- Fulbright, J. P. 2000, *AJ*, 120, 1841
- Fulbright, J. P. 2002, *AJ*, 123, 404
- Gilmore, G., Randich, S., Asplund, M., et al. 2012, *The Messenger*, 147, 25
- Gómez, F. A., Helmi, A., Brown, A. G. A., & Li, Y.-S. 2010, *MNRAS*, 408, 935
- Ibata, R. A., Gilmore, G., & Irwin, M. J. 1994, *Nature*, 370, 194
- Johnson, D. R. H. & Soderblom, D. R. 1987, *AJ*, 93, 864
- Kazantzidis, S., Bullock, J. S., Zentner, A. R., Kravtsov, A. V., & Moustakas, L. A. 2008, *ApJ*, 688, 254
- Lokas, E. L., Kazantzidis, S., & Mayer, L. 2011, *ApJ*, 739, 46
- Newberg, H. J., Yanny, B., Rockosi, C., et al. 2002, *ApJ*, 569, 245
- Nissen, P. E. & Schuster, W. J. 2010, *A&A*, 511, L10
- Read, J. I., Lake, G., Agertz, O., & Debattista, V. P. 2008, *MNRAS*, 389, 1041
- Reddy, B. E., Lambert, D. L., & Allende Prieto, C. 2006, *MNRAS*, 367, 1329
- Ruchti, G. R., Read, J. I., Feltzing, S., Pipino, A., & Bensby, T. 2014, *MNRAS*, 444, 515
- Ruchti, G. R., Read, J. I., Feltzing, S., et al. 2015, *ArXiv e-prints*

Schneider, P. 2015, *Extragalactic Astronomy and Cosmology: An Introduction*

Schönrich, R. 2012, *MNRAS*, 427, 274

Schönrich, R., Binney, J., & Dehnen, W. 2010, *MNRAS*, 403, 1829

Snaith, O., Haywood, M., Di Matteo, P., et al. 2014, *ArXiv e-prints*

Soubiran, C. & Girard, P. 2005, *A&A*, 438, 139

Steinmetz, M., Zwitter, T., Siebert, A., et al. 2006, *AJ*, 132, 1645

Suda, T., Yamada, S., Katsuta, Y., et al. 2011, *MNRAS*, 412, 843

Tolstoy, E., Hill, V., & Tosi, M. 2009, *ARA&A*, 47, 371

Tsujimoto, T., Nomoto, K., Yoshii, Y., et al. 1995, *MNRAS*, 277, 945

Appendix A

Matrix Calculations for velocities

The equations for the matrix calculations were taken from Johnson & Soderblom (1987). The matrix equation A.1 computes the U, V and W components of the velocity of a star. This requires: radial velocity v_r , parallax π , proper motion in right ascension μ_α , proper motion in declination μ_δ and a constant $k = 4.74047$.

$$\begin{bmatrix} U \\ V \\ W \end{bmatrix} = \mathbf{B} \cdot \begin{bmatrix} v_r \\ k\mu_\alpha/\pi \\ k\mu_\delta/\pi \end{bmatrix}. \quad (\text{A.1})$$

The matrix B is given by

$$\mathbf{B} = \mathbf{T} \cdot \mathbf{A}. \quad (\text{A.2})$$

$$\mathbf{T} = \begin{bmatrix} -0.0548755604 & -0.8734370902 & -0.4838350155 \\ 0.4941094279 & -0.4448296300 & 0.7469822445 \\ -0.8676661490 & -0.1980763734 & 0.4559837762 \end{bmatrix}. \quad (\text{A.3})$$

$$\mathbf{A} = \begin{bmatrix} \cos\alpha\cos\delta & -\sin\alpha & -\cos\alpha\sin\delta \\ \sin\alpha\cos\delta & \cos\alpha & -\sin\alpha\sin\delta \\ \sin\delta & 0 & \cos\delta \end{bmatrix}. \quad (\text{A.4})$$

To calculate uncertainties, a standard error propagation was used. The error propagation equation for the function given in A.5 is given by A.6. This was applied to equation A.1 to calculate the uncertainties in U, V and W, given in A.7.

$$f(x, y, z). \quad (\text{A.5})$$

$$\sigma_f^2 = \left(\frac{\partial f(x, y, z)}{\partial x} \sigma_x \right)^2 + \left(\frac{\partial f(x, y, z)}{\partial y} \sigma_y \right)^2 + \left(\frac{\partial f(x, y, z)}{\partial z} \sigma_z \right)^2. \quad (\text{A.6})$$

$$\begin{bmatrix} \sigma_U^2 \\ \sigma_V^2 \\ \sigma_W^2 \end{bmatrix} = \mathbf{C} \begin{bmatrix} \sigma_{v_r}^2 \\ (k/\pi)^2 [\sigma_{\mu_\alpha}^2 + (\mu_\alpha \sigma_\pi / \pi)^2] \\ (k/\pi)^2 [\sigma_{\mu_\delta}^2 + (\mu_\delta \sigma_\pi / \pi)^2] \end{bmatrix} + 2\mu_\alpha \mu_\delta k^2 \sigma_\pi^2 / \pi^4 \begin{bmatrix} b_{12} \cdot b_{13} \\ b_{22} \cdot b_{23} \\ b_{32} \cdot b_{33} \end{bmatrix}. \quad (\text{A.7})$$

Here, the matrix C is simply given by the square of each element of matrix B.